Landscapes as patches of plant functional types: An integrating concept for climate and ecosystem models

Gordon B. Bonan and Samuel Levis
National Center for Atmospheric Research, Boulder, Colorado, USA

Laurent Kergoat
National Center for Atmospheric Research, Boulder, Colorado, USA
Laboratoire d'Ecologie Terrestre, Toulouse, France

Keith W. Oleson
National Center for Atmospheric Research, Boulder, Colorado, USA

Received 16 October 2000; revised 13 March 2001; accepted 3 April 2001; published 22 May 2002.

[1] While most land models developed for use with climate models represent vegetation as discrete biomes, this is, at least for mixed life-form biomes, inconsistent with the leaf-level and whole-plant physiological parameterizations needed to couple these biogeophysical models with biogeochemical and ecosystem dynamics models. In this paper, we present simulations with the National Center for Atmospheric Research land surface model (NCAR LSM) that examined the effect of representing vegetation as patches of plant functional types (PFTs) that coexist within a model grid cell. This approach is consistent with ecological theory and models and allows for unified treatment of vegetation in climate and ecosystem models. In the standard NCAR LSM the PFT composition and leaf area for each grid cell are obtained by classifying grid cells as 1 of 28 possible biomes. Here, we develop a data set from 1-km satellite data that provides each model grid cell a unique PFT composition and leaf area for each PFT. Global simulations at $3^\circ \times 3^\circ$ spatial resolution showed that ground temperature, ground evaporation, and northern high-latitude winter albedo exhibited direct responses to these landscape changes, which led to indirect effects such as in soil moisture and sensible and latent heat fluxes. Additional simulations at $2^\circ \times 2^\circ$ and $1^\circ \times 1^\circ$ spatial resolution showed that low-resolution simulations masked landscape heterogeneity in both approaches but the satellite-based, continuous representation of vegetation reduced model sensitivity to resolution. It is argued that the use of spatially continuous distributions of coexisting PFTs is a necessary step to link climate and ecosystem models.
INDEX TERMS: 0315 Atmospheric Composition and Structure: Biosphere/atmosphere interactions

1. Introduction

[2] Land models such as Biosphere-Atmosphere Transfer Scheme (BATS) [*Dickinson et al.*, 1993] or simple biosphere (SiB) [*Sellers et al.*, 1996a] are the terrestrial component of climate models and simulate the exchanges of energy, water, and momentum between vegetation, soil, and the atmosphere. When coupled to climate models, they usually operate over coarse spatial resolution (e.g., 3° latitude by 3° longitude grid cells). Each grid cell is represented as one of several possible biomes or as multiple biomes when using subgrid mosaics. These biomes (Table 1) set vegetation characteristics such as albedo, roughness length, rooting depth, and stomatal physiology.

[3] The use of biomes is reasonable in a top-down modeling approach based on bulk parameterizations of grid cell fluxes of reflected solar radiation, sensible heat, latent heat, and surface stresses, biogeophysical fluxes typically required by atmospheric models. However, land surface models are expanding beyond their traditional biogeophysical roots to include biogeochemistry, especially photosynthesis and the carbon cycle [*Bonan*, 1995a; *Denning et al.*, 1995, 1996a, 1996b; *Foley et al.*, 1996; *Sellers et al.*, 1996a; *Craig et al.*, 1998; *Dickinson et al.*, 1998; *Cox et al.*, 1999; *Kucharik et al.*, 2000]. The ecological basis for this is the recognition that the physiology of stomata has evolved as a compromise between two conflicting goals, permitting carbon uptake during photosynthesis while restricting water loss during transpiration [*Cowan*, 1977]. These "third-generation" land surface models [*Sellers et al.*, 1997] explicitly link the physiology of stomata [e.g., *Collatz et al.*, 1991, 1992] to the biochemistry of leaf photosynthesis [e.g., *Farquhar et al.*, 1980].

[4] Inclusion of photosynthesis and the carbon cycle poses a problem with the biome-based land classification. How does one obtain the necessary leaf physiological and whole-plant allocation parameters for a biome? For monocultures this is relatively easy. Ecological parameters for a needleleaf evergreen tree are used for a needleleaf evergreen forest biome. For mixed life-form biomes this is more difficult. What is the photosynthetic light response curve of a savanna, which consists of physiologically distinct grasses and trees? Rooting depths also vary greatly between these life-forms. In grasslands, photosynthesis and stomatal conductance differ between C_3 and C_4 plants. Mixed forests are particularly difficult; trees differ not only in physiology but also in phenology. Tundra consists of mixtures of nonvascular plants, herbaceous plants, broadleaf deciduous shrubs, and needleleaf evergreen trees.

0886-6236/02/2000GB001360$12.00

Table 1. Three Vegetated Cover Types Available in IGBP DISCover[a]

SiB2	BATS	IGBP DISCover
Broadleaf evergreen tree	broadleaf evergreen tree	broadleaf evergreen forest
Broadleaf deciduous tree	broadleaf deciduous tree	broadleaf deciduous forest
Broadleaf and needleleaf trees	mixed woodland	mixed forest
Needleleaf evergreen tree	needleleaf evergreen tree	needleleaf evergreen forest
Needleleaf deciduous tree	needleleaf deciduous tree	needleleaf deciduous forest
Broadleaf shrub	evergreen shrub	closed shrub land
Dwarf trees and shrubs	deciduous shrub	open shrub land
Agriculture/C_3 grassland	tall grass (savanna)	woody savanna
Short vegetation/C_4 grassland	short grass	savanna
	tundra	grassland
	desert	cropland
	semidesert	crop and other vegetation
	cropland	barren or sparse
	irrigated crop	wetland
	wetland	snow and ice
	glacier	

[a] IGBP DISCover, International Geosphere-Biosphere Programme Data and Information System Global 1 km Land Cover Data Set [*Loveland et al.*, 2000].

[5] One solution is to recognize that biomes consist of individual species or plant functional types (PFTs) that do have measurable leaf physiology and carbon allocation. For example, the National Center for Atmospheric Research land surface model (NCAR LSM), considered to be a third-generation model [*Sellers et al.*, 1997], represents the vegetation in a grid cell as mixtures of 12 PFTs [*Bonan*, 1996]. Up to three PFTs can form distinct patches in a grid cell, with lakes and wetlands forming additional patches. Surface energy, water, and carbon fluxes are calculated separately for each patch.

[6] Ecologists developing physiologically based dynamic global vegetation models have wrestled with the same problem imposed by mixed life-form vegetation. Ecologists have long viewed landscapes as mosaics of vegetated patches with a structure and composition determined by site-specific microclimates, soils, geomorphology, and disturbance history [*Gleason*, 1926, , 1939; *Watt*, 1947; *Whittaker*, 1956; *Bormann and Likens*, 1979; *Shugart*, 1984]. Vegetation units such as associations or biomes are arbitrary products of classification rather than natural units clearly defined in the field [*Gleason*, 1926, 1939; *Whittaker*, 1956]. They are not emergent units, but are merely composed of plant species that coexist at a given point in space and time. As a result, plant functional types, which reduce the complexity of species diversity in ecological function to a few key plant types, are being advocated

Table 2. Surface Types and Associated PFTs and Fractional Cover Used in the Standard NCAR LSM[a]

	Patch 1		Patch 2		Patch 3	
Surface Type	PFT	Cover	PFT	Cover	PFT	Cover
Glacier	B	1.00	···	···	···	···
Desert	B	1.00	···	···	···	···
Needleleaf evergreen forest, cool	NET	0.75	B	0.25	···	···
Needleleaf deciduous forest, cool	NDT	0.50	B	0.50	···	···
Broadleaf deciduous forest, cool	BDT	0.75	B	0.25	···	···
Mixed forest, cool	NET	0.37	BDT	0.37	B	0.26
Needleleaf evergreen forest, warm	NET	0.75	B	0.25	···	···
Broadleaf deciduous forest, warm	BDT	0.75	B	0.25	···	···
Mixed forest, warm	NET	0.37	BDT	0.37	B	0.26
Broadleaf evergreen forest, tropical	BET	0.95	B	0.05	···	···
Broadleaf deciduous forest, tropical	TST	0.75	B	0.25	···	···
Savanna	WG	0.70	TST	0.30	···	···
Forest tundra, evergreen	NET	0.25	AG	0.25	B	0.50
Forest tundra, deciduous	NDT	0.25	AG	0.25	B	0.50
Forest crop, cool	C	0.40	BDT	0.30	NET	0.30
Forest crop, warm	C	0.40	BDT	0.30	NET	0.30
Grassland, cool	CG	0.60	WG	0.20	B	0.20
Grassland, warm	WG	0.60	CG	0.20	B	0.20
Tundra	ADS	0.30	AG	0.30	B	0.40
Shrub land, evergreen	ES	0.80	B	0.20	···	···
Shrub land, deciduous	DS	0.80	B	0.20	···	···
Semidesert	DS	0.10	B	0.90	···	···
Irrigated crop, cool	C	0.85	B	0.15	···	···
Crop, cool	C	0.85	B	0.15	···	···
Irrigated crop, warm	C	0.85	B	0.15	···	···
Crop, warm	C	0.85	B	0.15	···	···
Wetland, forest	BET	0.80	B	0.20	···	···
Wetland, nonforest	B	1.00	···	···	···	···

[a] NET, needleleaf evergreen tree; NDT, needleleaf deciduous tree; BET, broadleaf evergreen tree; BDT, broadleaf deciduous tree; TST, tropical seasonal tree; ES, evergreen shrub; DS, deciduous shrub; ADS, arctic deciduous shrub; CG, C_3 grass; WG, C_4 grass; AG, arctic grass; C, crop; B, bare.

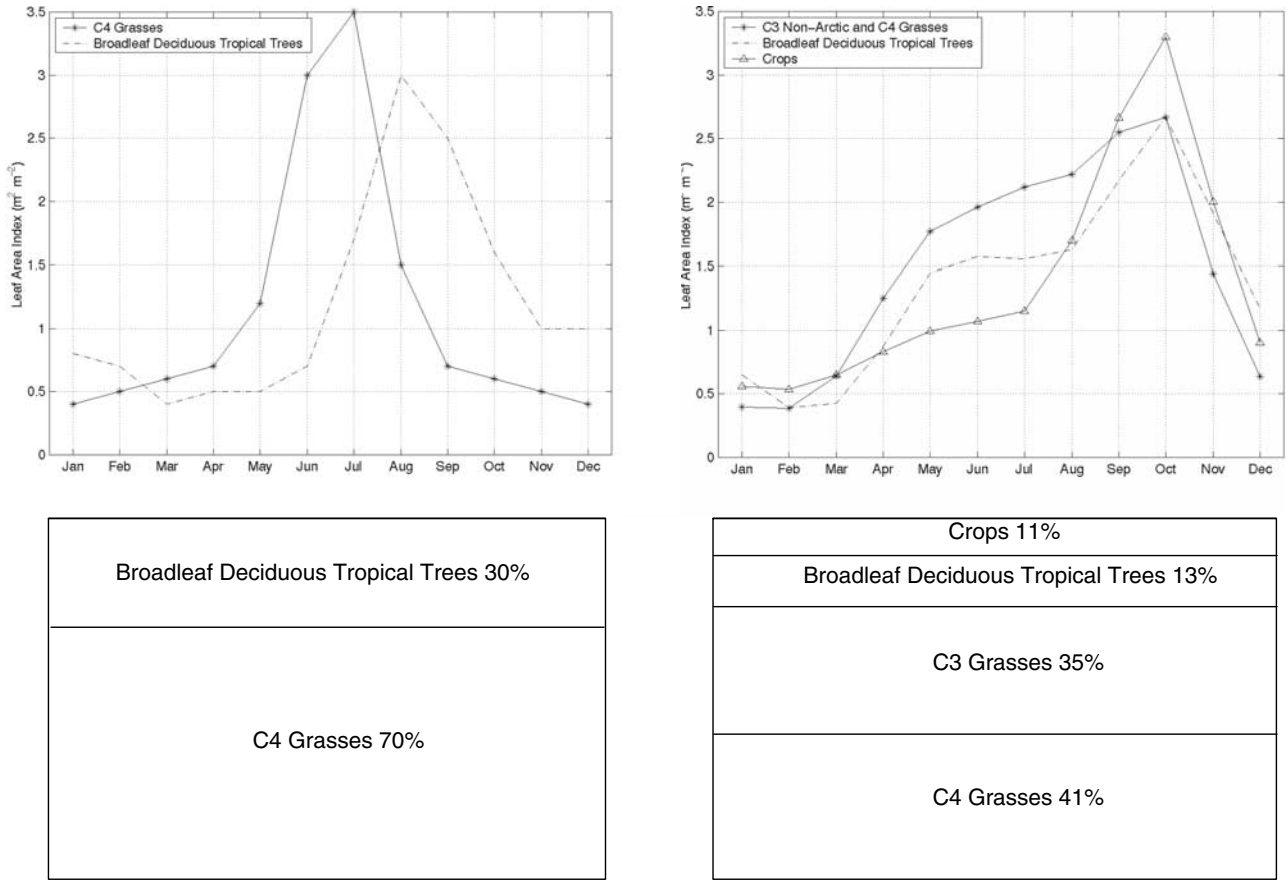

Figure 1. Composition and structure of vegetated patches in a grid cell. The figure shows, for a single grid cell centered on latitude 7.5°N and longitude 4.5°W, (top) the monthly leaf area index for each PFT patch and (bottom) the relative abundance of each PFT. The left panels show the fixed PFT LAI and PFT composition used in the biome data set of the standard model. The right panels show the new satellite-derived LAI and PFT composition for the same grid cell.

to predict the composition and functioning of ecosystems in a changing environment [*Woodward and Cramer*, 1996; *Smith et al.*, 1997]. Indeed, models of vegetation dynamics and biogeography routinely use PFTs [*Running and Coughlan*, 1988; *Running and Gower*, 1991; *Prentice et al.*, 1992; *Running and Hunt*, 1993; *Neilson*, 1995; *VEMAP members*, 1995; *Foley et al.*, 1996; *Haxeltine and Prentice*, 1996; *Schimel et al.*, 1997; *Kucharik et al.*, 2000].

[7] Representing the landscape as patches of PFTs is a common theme that can link climate and ecosystem models. It provides direct linkage to leaf-level ecophysiological measurements and ecological theory. In this paper, we explore the efficacy of the PFT approach in a land model for use with climate models. The NCAR LSM provides a convenient starting point because it already utilizes PFTs. However, the PFT composition of a grid cell is determined by 1 of 28 possible biomes (Table 2). For example, savanna grid cells consist of 70% C_4 grasses and 30% tropical trees (Figure 1). Furthermore, all C_4 grasses and all tropical trees follow a specified annual cycle of leaf area index (LAI). All needleleaf evergreen forests, excluding wetland and lake patches,

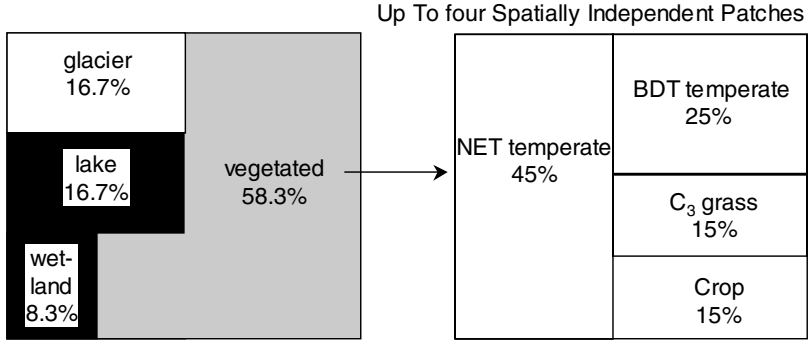

Figure 2. Subgrid patches of glacier, lake, wetland, and vegetation in the new version of the NCAR LSM. The vegetated portion of the grid cell is divided into up to four PFTs with unique composition and leaf area.

Table 3. Plant Functional Types and Their Derivation From 1-km Land Cover Data and Climate Rules[a]

Plant Functional Type	1-km Land Cover Data	Climate Rules
Needleleaf evergreen tree, temperate	needleleaf evergreen tree	$T_c > -19$°C and GDD > 1200
Needleleaf evergreen tree, boreal	needleleaf evergreen tree	$T_c \leq -19$°C or GDD $\leq$ 1200
Needleleaf deciduous tree	needleleaf deciduous tree	none
Broadleaf evergreen tree, tropical	broadleaf evergreen tree	$T_c > 15.5$°C
Broadleaf evergreen tree, temperate	broadleaf evergreen tree	$T_c \leq 15.5$°C
Broadleaf deciduous tree, tropical	broadleaf deciduous tree	$T_c > 15.5$°C
Broadleaf deciduous tree, temperate	broadleaf deciduous tree	-15°C $< T_c \leq 15.5$°C and GDD > 1200
Broadleaf deciduous tree, boreal	broadleaf deciduous tree	$T_c \leq -15$°C or GDD $\leq$ 1200
Broadleaf evergreen shrub, temperate	shrub	$T_c > -19$°C and GDD > 1200 and $P_{ann} > 520$ mm and $P_{win} > 2/3\ P_{ann}$
Broadleaf deciduous shrub, temperate	shrub	$T_c > -19$°C and GDD > 1200 and ($P_{ann} \leq 520$ mm or $P_{win} \leq 2/3\ P_{ann}$)
Broadleaf deciduous shrub, boreal	shrub	$T_c \leq -19$°C or GDD $\leq$ 1200
C_3 grass, arctic	grass	GDD < 1000
C_3 grass[b]	grass	GDD > 1000 and ($T_w \leq 22$°C or $P_{mon} \leq 25$ mm and for months with $T > 22$°C)
C_4 grass[b]	grass	GDD > 1000 and $T_c > 22$°C and driest month $P_{mon} > 25$ mm
Crop	crop	none

[a] T_c, temperature of coldest month. T_w, temperature of warmest month. GDD, growing-degree days above 5°C. P_{ann}, annual precipitation. P_{win}, winter precipitation (Northern Hemisphere, November through April; Southern Hemisphere, May through October). P_{mon}, monthly precipitation.
[b] A 1-km grid cell is assumed to be 50% C_3 and C_4 if GDD > 1000 and neither the C_3 nor C_4 criteria are met.

are 25% bare ground and 75% needleleaf evergreen tree; and all needleleaf evergreen trees have a height of 17 m, a maximum LAI of 5, and a minimum LAI of 4. The use of biomes to set PFT composition and structure homogenizes a heterogeneous land cover.

[8] The advent of high-spatial-resolution (e.g., 1 km) satellite land cover and LAI products allows us to expand on the existing PFT construct by separating vegetation composition (i.e., the number of PFTs and their abundance) from stand structure (e.g., LAI) and to provide a unique composition and structure for each grid cell (Figure 1). *Oleson and Bonan* [2000] explored this for boreal forests, representing the landscape as a continuous mosaic of coexisting physiologically distinct plants rather than as biomes. In this paper, we use global 1-km land cover and vegetation reflectance data sets, both based on advanced very high resolution radiometer (AVHRR), to develop and test a similar methodology for climate models.

2. Methods

[9] The original 12 PFTs used with the standard NCAR LSM were expanded to 15 to better match those used in dynamic global vegetation models. The geographic distribution and abundance of these 15 PFTs were derived from 1-km land cover and tree cover data sets using climate-based rules to define ecological variants of the principal PFTs. This is in contrast to the standard biome-based version of the model, in which the abundance of PFTs is defined by classifying the grid cell as 1 of 28 possible biomes (Table 2). In addition, monthly leaf area index for each PFT in each grid cell was created from the AVHRR archive to derive a more realistic phenology and to allow for spatial variability in the amount of leaves. This is in contrast to the standard model's prescribed monthly phenology for each PFT [*Dorman and Sellers*, 1989] and differs from previous LAI data products that classified grid cells into one of several biomes and derived a grid-average LAI [*Myneni et al.*, 1997; *Knyazikhin et al.*, 1998a, 1998b; *Sellers et al.*, 1994, 1996b; *Randall et al.*, 1996]. The model was run for two 20-year simulations, forced with prescribed atmospheric data, using the original biome-derived PFTs of the standard model and the satellite-derived PFTs of the new model. Simulations were repeated for 1° × 1°, 2° × 2°, and 3° × 3° global horizontal resolutions to evaluate the sensitivity of each approach to spatial resolution.

2.1. Model Description

[10] The NCAR LSM simulates the exchange of energy, water, momentum, and carbon between the surface and the atmosphere [*Bonan*, 1996]. Vegetation effects are included by allowing for several PFTs that differ in leaf and stem areas, root profile, height, leaf dimension, optical properties, stomatal physiology, roughness length, displacement height, and biomass. In the standard model, 12 PFTs form 28 different biomes, each composed of multiple plant types and bare ground so that, for example, a mixed broadleaf deciduous and needleleaf evergreen forest consists of patches of broadleaf deciduous trees, needleleaf evergreen trees, and bare ground. The types of biomes (Table 2) and their geographic distributions are based on *Olson et al.* [1983]. Each patch, while co-occurring in a grid cell, is a separate column upon which energy, water, and carbon calculations are performed. Thus PFTs do not compete for light and water. Lakes and wetlands, if present, form additional patches.

Table 4. Minimum and Maximum NDVI and Corresponding Minimum and Maximum LAI

	NDVI		LAI	
Plant Functional Type	Minimum	Maximum	Minimum	Maximum
Needleleaf evergreen tree	0.1	0.6342	0.1	5
Needleleaf deciduous tree	0.1	0.6197	0	5
Broadleaf evergreen tree	0.1	0.6533	0.1	7
Broadleaf deciduous tree	0.1	0.6561	0	5
Shrub	0.1	0.4726	0	4
Grass	0.1	0.5636	0	4
Crop	0.1	0.5591	0	4

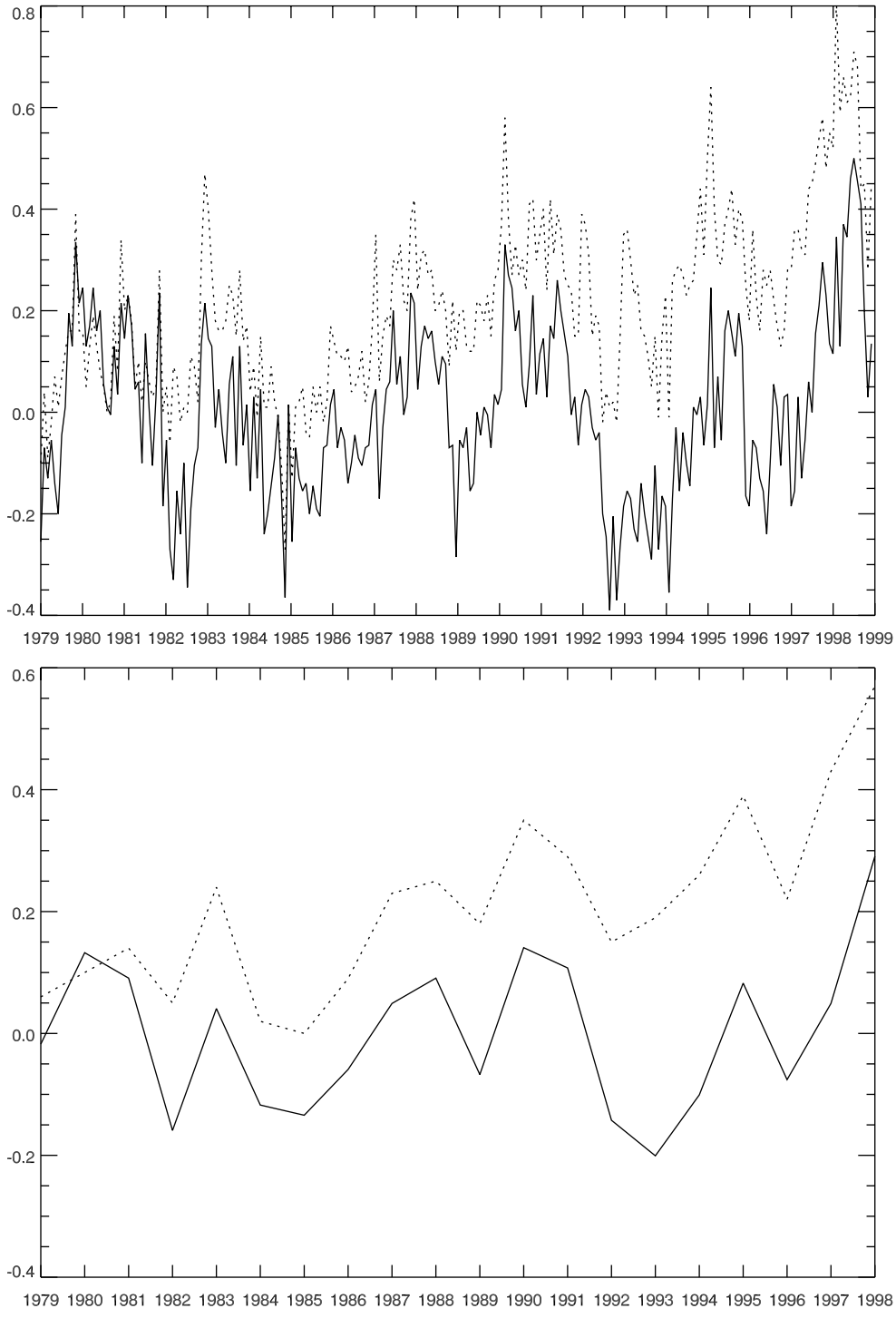

Figure 3. Global (top) monthly and (bottom) annual temperature anomalies (degrees Celsius). *Jones et al.* [1999] anomalies (dotted lines) are relative to the 1961–1990 mean. The anomalies for the atmospheric forcing used in this study (solid lines) are relative to the 1979–1998 mean.

[11] Soil effects are included by allowing thermal and hydraulic properties to vary depending on sand and clay content. Soils also differ in color, which affects soil albedo. Consequently, each grid cell is assigned a biome type (which determines the patch fractions for each PFT), the fraction of the grid cell covered by lakes, the fraction covered by wetlands, soil texture (percent sand, silt, and clay), and soil color.

[12] *Bonan* [1996] documents the model, and *Bonan* [1998] describes the climatology of the model coupled to the Community Climate Model. Comparisons with tower flux data show that the model reasonably simulates surface fluxes at several boreal forest [*Bonan et al.*, 1997] and tundra [*Lynch et al.*, 1999] sites. The model has been used to study land-atmosphere CO_2 exchange [*Bonan*, 1995a; *Craig et al.*, 1998], the effect of lakes and wetlands

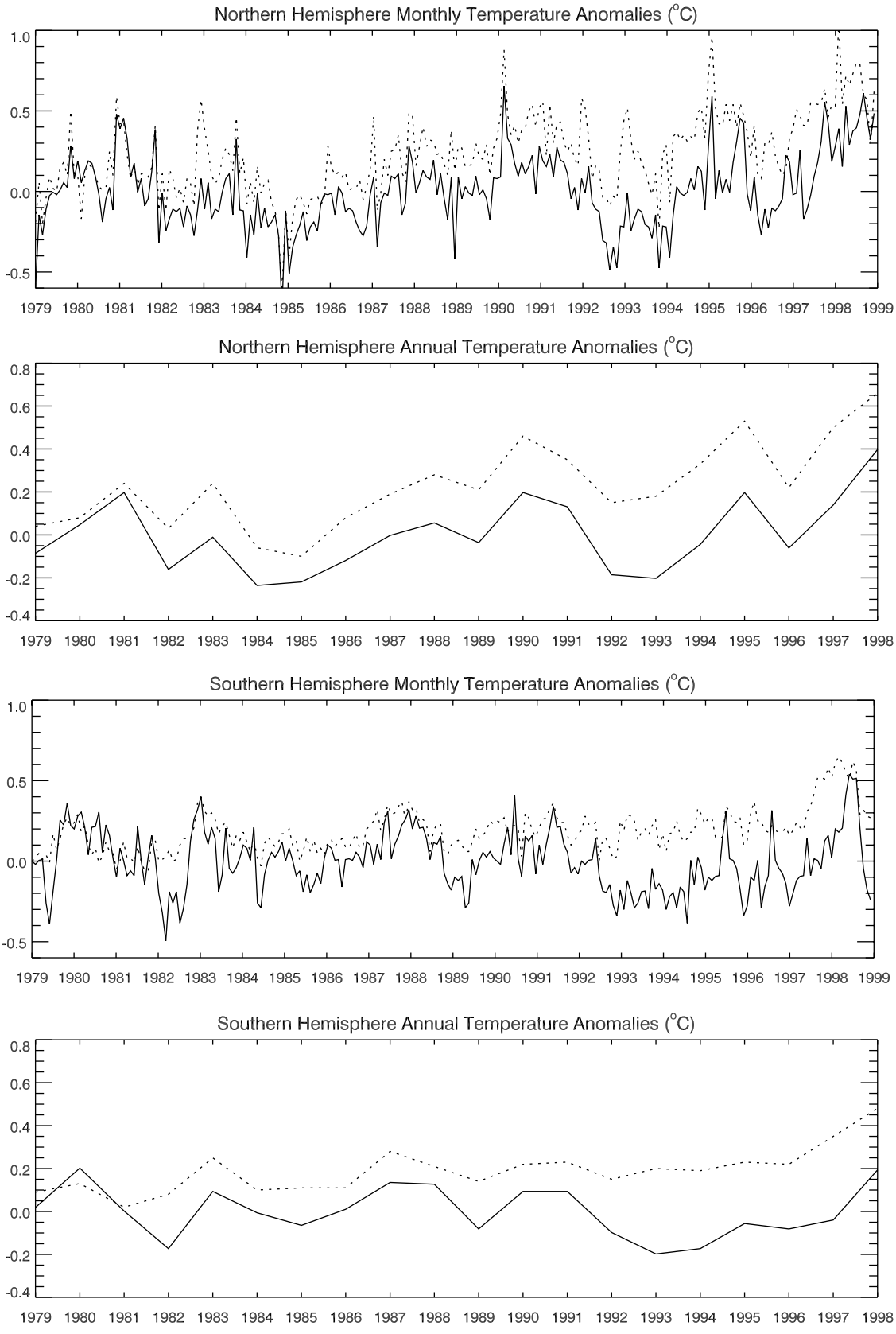

Figure 4. Northern and Southern Hemisphere monthly and annual temperature anomalies (degrees Celsius). *Jones et al.* [1999] anomalies (dotted lines) are relative to the 1961–1990 mean. The anomalies for the atmospheric forcing used in this study (solid lines) are relative to the 1979–1998 mean.

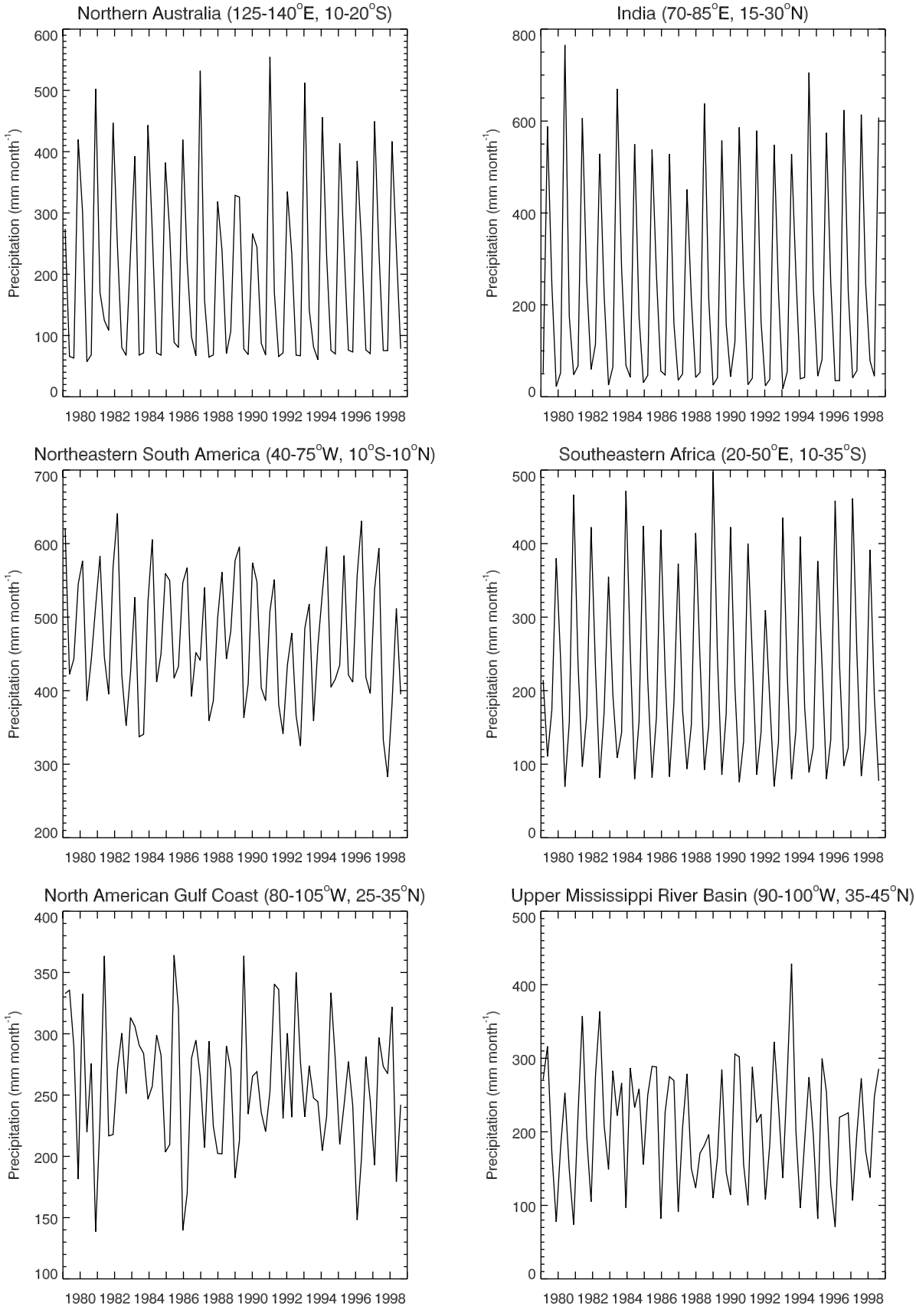

Figure 5. Seasonal precipitation totals for selected regions for the atmospheric forcing used in this study.

Table 5. Precipitation Totals for Selected Regions During El Niño and La Niña[a]

Region and Season	Latitude and Longitude	Atmospheric Forcing			*Ropelewski and Halpert* [1996]		
		Base	El Niño	La Niña	Base	El Niño	La Niña
Northeastern South America, July–March	40°–75°W, 10°S to 10°N	1261	1213	1531	1100	940	1190
India, June–September	70°–85°E, 15°–30°N	680	650	812	705	635	755
Southeastern Africa, November–April	20°–50°E, 10°–35°S	639	604	762	665	605	725
Northern Australia, September–January	125°–140°E, 10°–20°S	291	277	351	520	410	665

[a] The base period for the atmospheric forcing is 1979–1998. The base period for *Ropelewski and Halpert* [1996] is 1901–1992, except for South America (1938–1992). Precipitation totals are given in millimeters.

on climate [*Bonan*, 1995b], the effect of vegetation and soil [*Kutzbach et al.*, 1996] and lakes and wetlands [*Coe and Bonan*, 1997] on the African monsoon in the middle Holocene, the effect of soil water on floods and droughts in the Mississippi River basin [*Bonan and Stillwell-Soller*, 1998], the effect of tundra ecosystems on arctic climate [*Lynch et al.*, 1999], and the effects of temperate deforestation on climate [*Bonan*, 1997, 1999].

[13] For this study, the model was reformulated so that landscapes consist of statistical distributions of four types of patches (glacier, lake, wetland, vegetated) within a grid cell (Figure 2). This is in contrast to the standard biome approach (Table 2), in which glaciers are considered as one of the 28 possible biomes and wetlands, in addition to being a subgrid patch, are also defined as two biomes (forest wetland, nonforest wetland). For the new satellite-based simulations, glaciers and wetlands exist only as patches within a grid cell. The glacier patches were obtained from the 1-km International Geosphere-Biosphere Programme Data and Information System Global 1 km Land Cover Data Set (IGBP DISCover) [*Loveland et al.*, 2000]. Lake and wetland patches were obtained as previously [*Bonan*, 1995b, 1996]. The vegetated portion of a grid cell is further divided into a statistical distribution of patches of 4 of 15 PFTs with corresponding leaf area index, stem area index, and height (Figure 2). Physiological parameters for the 15 PFTs were obtained from the 12 original PFTs [*Bonan*, 1996] so that although the list of PFTs expanded, no new physiologies were introduced. Stem area index and height were based on the original values prescribed for each PFT [*Bonan*, 1996].

[14] The original NCAR LSM allowed for two irrigated crop biomes (Table 2) whereas the satellite-derived PFTs only recognize a crop plant. To minimize differences with the biome-based depiction of PFTs, a separate irrigation data set was created at 0.5° by 0.5° from the original NCAR LSM biomes. Crop PFT patches were irrigated during the growing season if they were located in an irrigated grid cell.

2.2. Plant Functional Type Data Set

[15] Fifteen PFTs were defined based on available 1-km land cover data and climate rules (Table 3). The seven primary PFTs are needleleaf evergreen or deciduous tree, broadleaf evergreen or deciduous tree, shrub, grass, and crop. These are adapted from the logic of *Running et al.* [1995], who suggested six PFTs (needleleaf and broadleaf evergreen perennial, needleleaf and broadleaf deciduous perennial, broadleaf annual, and grass) using a classification based on permanence of aboveground biomass, leaf longevity, and leaf type. These characteristics are observable by remote sensing and are key ecological properties determining stomatal conductance, photosynthesis, and carbon allocation. Subsequently, *Nemani and Running* [1996] suggested that these six PFTs be expanded to allow for physiological variants on the basis of simple climate rules.

[16] One-half-degree maps of the abundance of each primary PFT were derived from the 1-km IGBP DISCover data set [*Loveland et al.*, 2000] of natural and anthropogenic land cover (Table 1) and the 1-km University of Maryland tree cover data set [*DeFries et al.*, 1999, 2000a, 2000b] of evergreen, deciduous, broadleaf, and needleleaf tree cover. Each 1-km pixel was assigned the percentage of needleleaf evergreen, needleleaf deciduous, broadleaf evergreen, and broadleaf deciduous trees as given in the tree cover data. Where the tree cover data showed that a pixel was exclusively broadleaf or needleleaf, the deciduous and evergreen tree cover determined the appropriate leaf longevity. Where the tree cover data showed that a pixel was exclusively evergreen or deciduous, the broadleaf and needleleaf tree cover determined the appropriate leaf type. In the rare occasion that all four categories were present, we assumed that needleleaf deciduous trees (a boreal plant type) could not coexist with broadleaf evergreen trees (a tropical or temperate type). In particular, in regions where needleleaf deciduous trees could not exist, the needleleaf percentage had to be needleleaf evergreen trees, and the deciduous percentage had to be broadleaf deciduous trees. The difference between the evergreen percentage and the needleleaf evergreen percentage should then equal the percent of broadleaf evergreens. Similarly, in regions where broadleaf evergreen trees could not exist, the broadleaf percentage had to be broadleaf deciduous trees, and the evergreen percentage had to be needleleaf evergreen trees. The difference between the deciduous percentage and the broadleaf deciduous trees should equal the percent of needleleaf deciduous trees.

[17] The non-tree-covered portion of the 1-km pixel was determined from the IGBP DISCover data. In this data set, bare ground originates from nonvegetated land (“barren or sparsely vegetated” land cover) and may not be present even in semiarid regions with sparse, yet homogeneous land cover. Because we lacked consistent information on nonvegetated cover, we assumed that non-tree-covered land in forests, savannas, and grasslands was covered by grasses, in shrub lands by shrubs, in croplands by crops. Other IGBP cover types were treated as bare ground. This is different from the biome-based implementation of the NCAR LSM (Table 2), where bare ground is always present as a subgrid patch and is considered to be the cumulative canopy openings in a grid cell.

[18] The 1-km data were converted from their Goode Homolosine projection to a 0.5° by 0.5° grid by finding the latitude and longitude of every 1-km grid cell [*Steinwand*, 1994] and averaging the 1-km percentages per 0.5° grid cell. This procedure normalized the percent of each grid cell covered by a particular PFT by the vegetated area (i.e., excluding the IGBP DISCover water, urban, snow-ice, and wetland land cover types).

[19] The 7 primary PFTs were expanded to 15 physiological variants based on climate rules. *Nemani and Running* [1996] suggested using absolute minimum temperature to determine tropical, subtropical, temperate, and boreal varieties. Additional varieties were possible on the basis of water availability. Instead, we used temperature- and precipitation-based rules that limit the geographic distribution of PFTs in the Global biome model (BIOME) [*Prentice et al.*, 1992; *Haxeltine and Prentice*, 1996] and Integrated Biosphere Simulator (IBIS) [*Foley et al.*, 1996] terrestrial biosphere models, supplemented by discrimination of C_3 and C_4 grasses [*Collatz et al.*, 1998] and Mediterranean shrub land [*Keeley and Keeley*, 1988], to distinguish arctic, boreal, temperate,

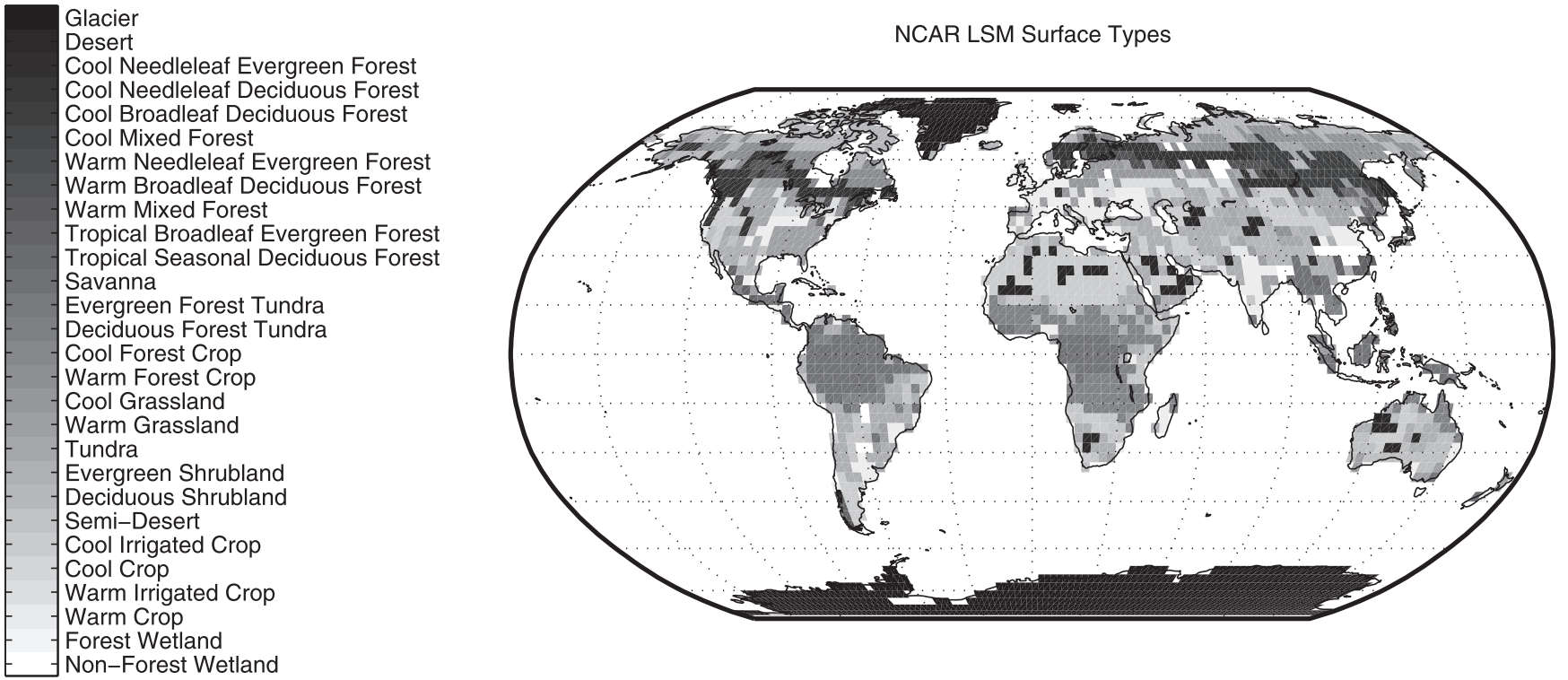

Figure 6. Biome types represented in the NCAR LSM. See color version of this figure at back of this issue.

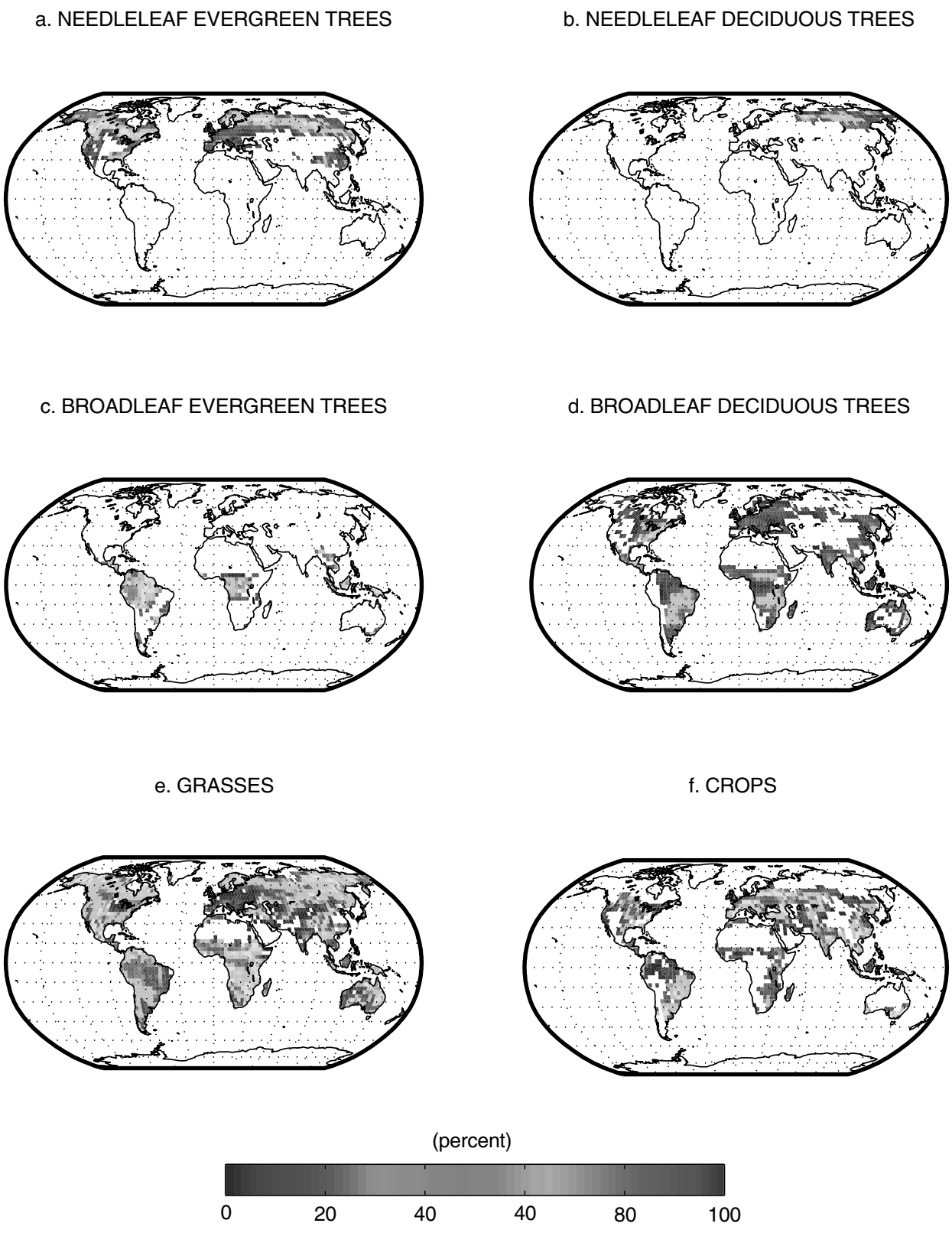

Figure 7. Distribution of (a) needleleaf evergreen trees, (b) needleleaf deciduous trees, (c) broadleaf evergreen trees, (d) broadleaf deciduous trees, (e) grasses, and (f) crops on a $3^\circ \times 3^\circ$ grid. Maps show the percent of the grid cell occupied by each plant type. See color version of this figure at back of this issue.

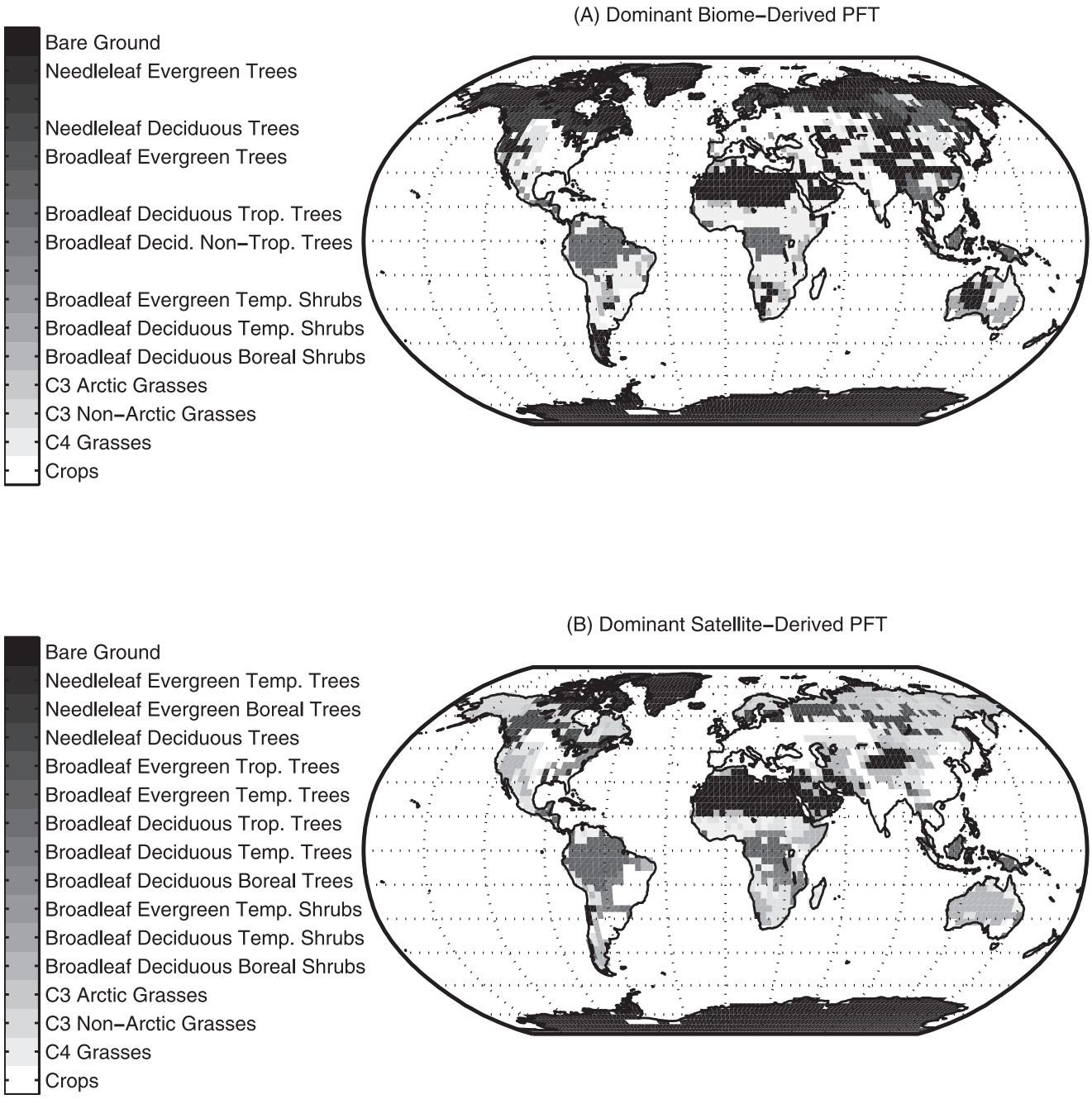

Figure 8. Dominant plant functional types. (a) Biome data set. (b) Satellite data set. See Table 3 for a definition of the PFTs. See color version of this figure at back of this issue.

and tropical PFTs, C_3 and C_4 grasses, and evergreen and deciduous shrubs (Table 3). The 0.5° by 0.5° *Legates and Willmott* [1990a, 1990b] temperature and precipitation climatology was used. Needleleaf evergreen trees were distinguished as temperate or boreal on the basis of whether the temperature of the coldest month is greater than −19°C and growing-degree days exceed 1200. Broadleaf evergreen trees were either tropical or temperate based on coldest monthly temperature of 15.5°C. Broadleaf deciduous trees were tropical, temperate, or boreal. Shrubs were temperate if the temperature of the coldest month is above −19°C and growing-degree days exceed 1200; the rest were boreal. Temperate shrubs were distinguished as evergreen or deciduous on the basis of the seasonal distribution of precipitation. Where annual precipitation exceeds 520 mm and more than two thirds of the annual rainfall is in winter, a characteristic of Mediterranean vegetation [*Keeley and Keeley*, 1988], the shrubs were evergreen. Grasses were separated into arctic and nonarctic varieties on the basis of a growing-degree days threshold of 1000. Nonarctic grasses were distinguished as C_3 or C_4 on the basis of the temperature of the warmest month and precipitation so that the abundance of C_4 grasses increases in warmer and wetter climates [*Collatz et al.*, 1998].

2.3. Leaf Area Index Data Set

[20] Thirty-six global images of 1-km AVHRR red and near-infrared reflectances (channels 1 and 2) for April 1992 to March

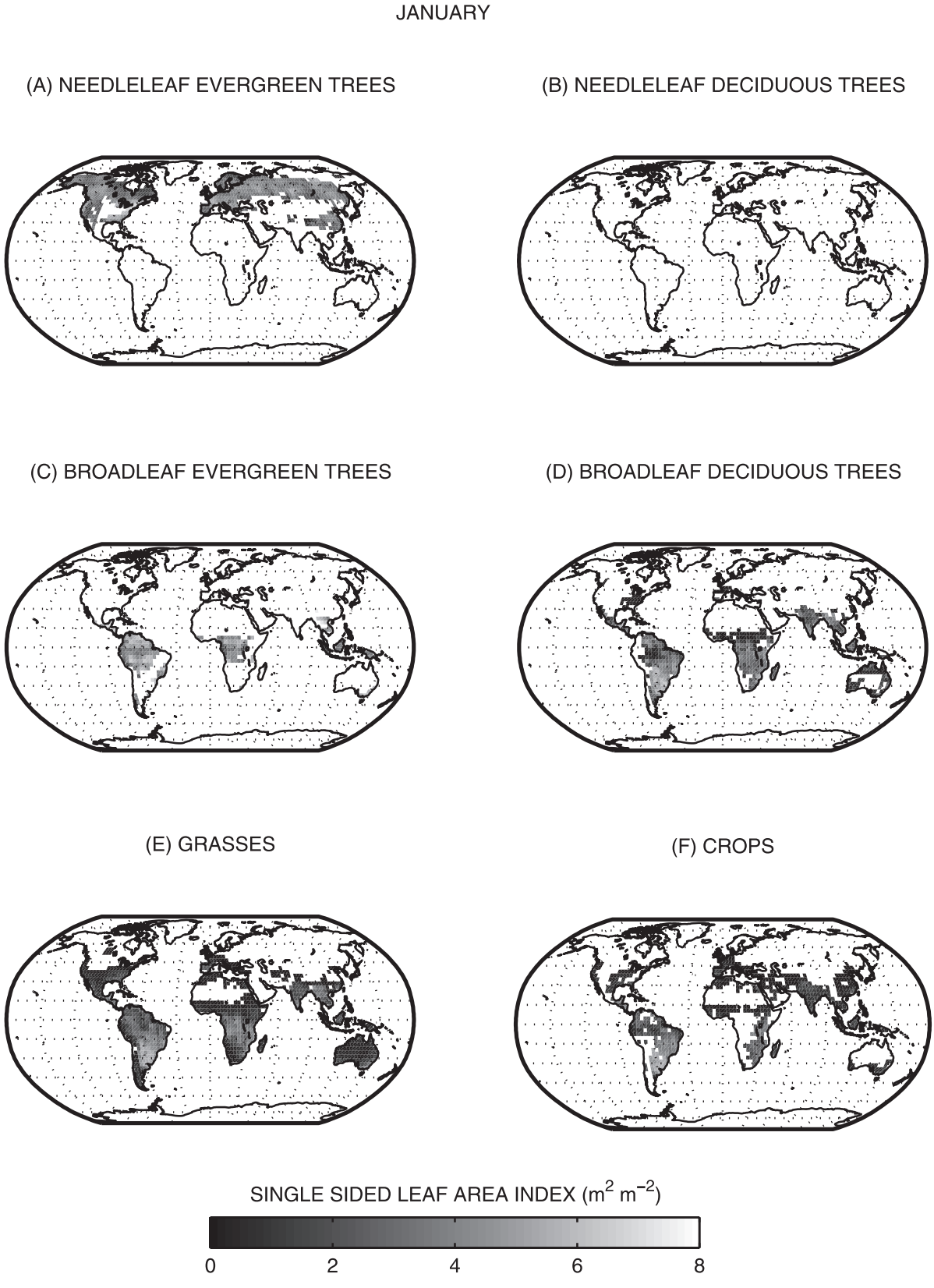

Figure 9. January satellite-derived leaf area index for (a) needleleaf evergreen trees, (b) needleleaf deciduous trees, (c) broadleaf evergreen trees, (d) broadleaf deciduous trees, (e) grasses, and (f) crops on a $3^\circ \times 3^\circ$ grid. See color version of this figure at back of this issue.

1993 were obtained from the U.S. Geological Survey Earth Resources Observation System (EROS) Data Center Distributed Active Archive Center (DAAC) [*Eidenshink and Faundeen*, 1994; *DeFries et al.*, 2000b]. These data were used to derive the seasonal course of LAI for every PFT present in a 200-km by 200-km grid cell. This choice of resolution assumes that canopy phenology does not vary appreciably at scales less than 200 km while allowing for a high number of 1-km pixels to statistically reduce the noise inherent to satellite data. The specific time period was chosen because it corresponds to the period used to construct the tree cover maps. First, a "pure PFT" normalized difference vegetation index (NDVI) temporal profile was derived for each 200-km by 200-km grid cell. The NDVI profile was then converted to a LAI profile. Then, the 200-km LAI product was interpolated to a 0.5° by 0.5° grid.

[21] The "pure PFT" NDVI was derived from the 1-km AVHRR reflectances and the abundance of the seven primary PFTs (needleleaf evergreen tree, needleleaf deciduous tree, broadleaf evergreen tree, broadleaf deciduous tree, shrub, grass, and crop) and bare ground for each 1-km pixel. For each PFT present in a 200-km grid cell the pure PFT NDVI was extracted by averaging the NDVI over 1-km pixels in which the abundance of the PFT was greater than 60%. An alternative method based on linear unmixing used every 1-km pixel with its corresponding PFT abundances. While this method is theoretically preferable, the results from the first approach were more robust and were used to derive LAI.

[22] Two filters were applied on a pixel by pixel basis (200-km by 200-km grid) for all 36 dates in the NDVI time series to remove outliers and cloud-biased data. The first filter was applied to discard isolated peaks in the NDVI time profile. These data are spurious or may be caused by cloud shadows that produce artificially high NDVI. Very few data values were actually discarded in this filtering. The second filter was applied to discard cloud-biased data, which have low NDVI. This filter is based on the best index slope extraction (BISE) method [*Viovy et al.*, 1992] and is a refined "maximum value composite" that keeps a better time resolution.

[23] Smooth growing season and leaf senescence periods were obtained by fitting the NDVI profile with analytical functions. The growing period (increasing NDVI) and senescence period (decreasing NDVI) were fitted separately. The functions were chosen to allow for plateaus of maximum and minimum NDVI and rapid or slow change between the minimum and maximum NDVI. The NDVI temporal profile was adjusted to ensure consistency with the PFT. For example, a deciduous PFT must break buds at the beginning of the growing season and drop leaves at the end of the growing season. To account for this, we assumed that the minimum NDVI corresponds to a LAI of zero for deciduous PFTs. Evergreen PFTs retain leaves year-round. For evergreen PFTs we assumed that the minimum NDVI corresponds to 75% of the maximum LAI (or the computed NDVI minimum LAI if it was larger). This allowed for some phenology rather than forcing a constant LAI year-round. It also improved results for boreal forests, which have very low NDVI in winter because of snow cover and low or no light. Similarly, this formulation improved the results for tropical evergreen vegetation, which also shows low-NDVI periods caused by persistent cloud cover. For crops, grasses, and shrubs the minimum NDVI was unconstrained and produced either deciduous or semi-deciduous LAI temporal profiles.

[24] The NDVI profiles were converted to LAI using an approximation of the NDVI-LAI relationships of *Myneni et al.* [1997]. The derived relationships are PFT-dependent hyperbolas defined by the slope at the origin, an asymptote for high LAI values, and a shape parameter. These quantities were estimated from *Myneni et al.* [1997, Figure 5a]. Because the NDVI data set generated by *Myneni et al.* [1997] and the one used in this study are different in terms of radiometric and atmospheric correction, the slope and asymptote were adjusted to match the maximum NDVI with a prescribed maximum LAI and to match the minimum NDVI with a minimum LAI. For each PFT the maximum NDVI was computed as the mean for the upper 98–99.5% of the NDVI histogram. The minimum NDVI was set to the average value for desert areas (0.1). The minimum LAI was set to zero for all PFTs except evergreen PFTs, for which it was set to 0.1 (Table 4). For a PFT which was present in a 200-km cell but never exceeded the 60% threshold in any corresponding 1-km pixel we did not get a "pure PFT" NDVI. Such gaps were filled by taking the LAI profile from the nearest neighboring grid cell containing the same PFT.

2.4. Atmospheric Data Set

[25] A global, multiyear 3-hour atmospheric forcing data set at T62 spatial resolution (approximately 1.875° longitude by 1.915° latitude) was created for the period 1979–1998 from the National Center for Environmental Prediction (NCEP) reanalysis project [*Kalnay et al.*, 1996]. Observations of precipitation [*Xie and Arkin*, 1997] and downwelling surface solar radiation [*Bishop et al.*, 1997], regridded from their original 2.5° grids to the NCEP T62 grid, were used to correct for deficiencies in these variables in the NCEP reanalysis. Instantaneous temperature, wind speed, specific humidity, and surface pressure at 6-hour resolution were extracted from the reanalyses and linearly interpolated to 3-hour resolution. Infrared radiation emitted by the atmosphere was calculated from air temperature and water vapor [*Idso*, 1981]. Precipitation, which was averaged over the 6-hour interval, was applied uniformly to the two corresponding 3-hour intervals. Precipitation rates were scaled to the observed monthly precipitation totals of *Xie and Arkin* [1997]. The frequency of precipitation was not corrected because of insufficient data to correctly match daily and hourly rain events during the 1979–1998 period. Surface solar radiation was obtained from top of the atmosphere solar radiation scaled to match a 1984–1990 climatology of monthly surface solar radiation from the International Satellite Cloud Climatology Project [*Bishop et al.*, 1997]. Monthly atmospheric attenuation factors were obtained based on monthly top of the atmosphere solar radiation and observed surface solar radiation. The attenuation factors were applied to hourly top of the atmosphere solar radiation to produce 3-hour surface solar radiation.

[26] When compared with *Jones et al.* [1999], there is good correlation between the global monthly and annual temperature anomalies ($r = 0.7$ for both monthly and annual anomalies) over the 20-year period (Figure 3). Similarly, the Northern Hemisphere anomalies (Figure 4) show good correlation (monthly, $r = 0.8$; annual, $r = 0.9$). The Southern Hemisphere anomalies are not as well correlated (monthly, $r = 0.5$; annual, $r = 0.4$). Time series of seasonal precipitation totals for selected regions show substantial seasonal and interannual variability captured in the precipitation field (Figure 5). For example, precipitation differences in the upper Mississippi River basin in the drought and flood years of 1988 and 1993, respectively, are clearly evident in the data set. For other regions the precipitation is linked with the phases of the El Niño–Southern Oscillation as supported by observations [*Ropelewski and Halpert*, 1996]. Total precipitation for selected regions and seasons declined during El Niño and increased during La Niña compared to the base period (Table 5). The decrease in precipitation during El Niño is likely not as great as in the observations because the period after 1979 has been biased warm and dominated by El Niño events [*Trenberth and Hoar*, 1996]. The increase in precipitation during La Niña is likely greater than in the observations because only one La Niña event was used (1988) to calculate the precipitation totals. The 1988 La Niña was one of the strongest in the past 50 years [*Trenberth*, 1997].

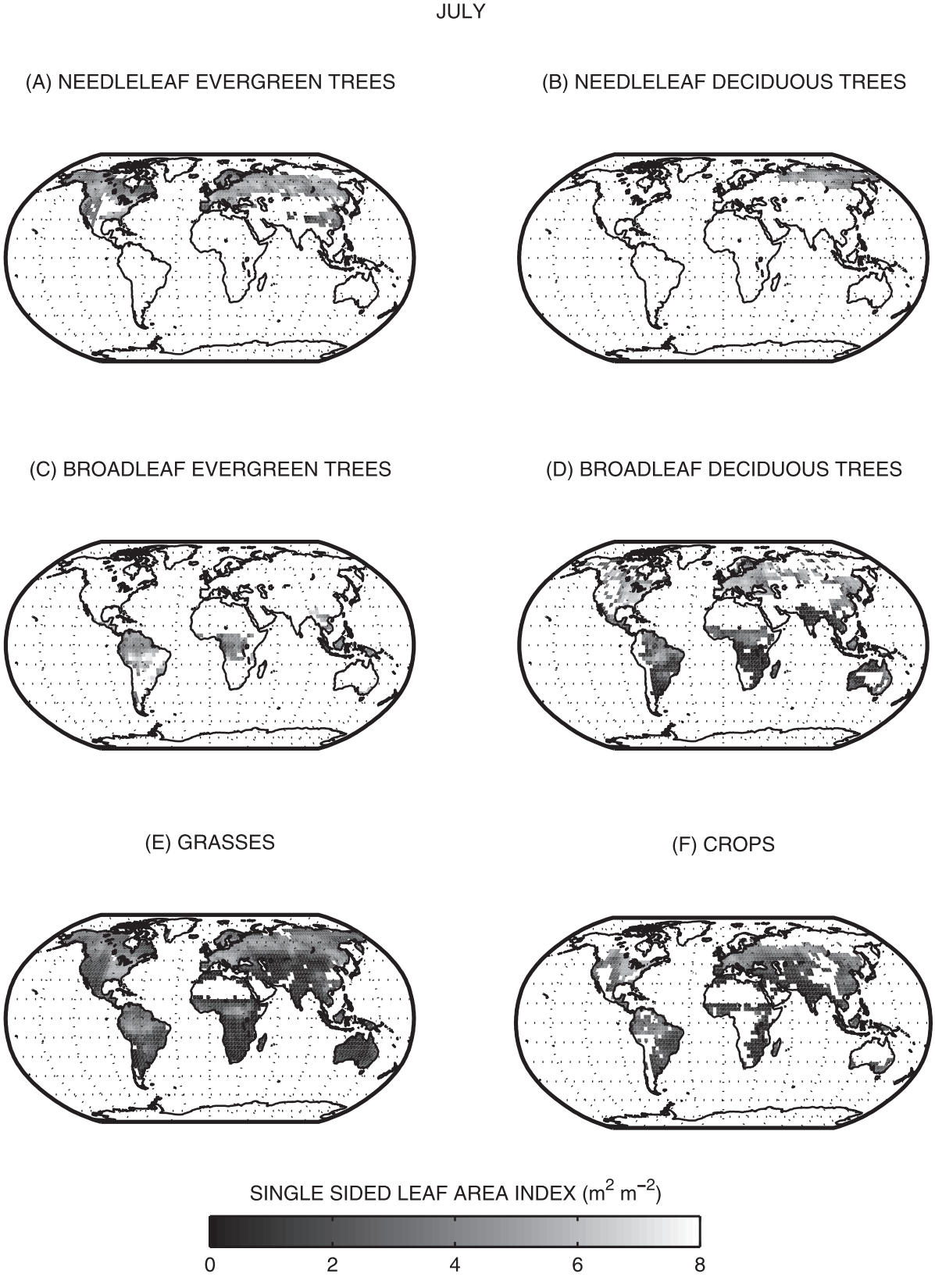

Figure 10. July satellite-derived leaf area index for (a) needleleaf evergreen trees, (b) needleleaf deciduous trees, (c) broadleaf evergreen trees, (d) broadleaf deciduous trees, (e) grasses, and (f) crops on a $3^\circ \times 3^\circ$ grid. See color version of this figure at back of this issue.

[27] We recognize potential meteorological inconsistencies in our approach. In particular, the approach does not preserve temporal correlations among temperature, solar radiation, humidity, and rainfall. At best, the data set is a "pseudo-realistic" climate forcing, but it is likely a more accurate representation of the 1979–1998 period than data from stochastic weather generators and preserves the interannual variability important for our studies. Data were regridded from the T62 grid to the appropriate model resolution using a simple area-averaging approach [*Hahmann and Dickinson*, 2001].

3. Results

3.1. Plant Functional Types

[28] The biome-based classification (Figure 6) homogenizes the land surface compared to continuous PFT abundances (Figure 7). For example, any grid cell that is considered savanna in the biome data set is composed of two patches: Trees cover 30% of the grid cell, and C_4 grasses cover 70% (Figure 1). The new PFT data set shows that one such grid cell classified as savanna actually consists of 76% C_3 and C_4 grasses, 13% tree, and 11% crop. In many regions the dominant PFT differs between the two approaches (Figure 8). Some of these differences occur because of the different definition for bare ground used in the biome-based approach versus the satellite-based approach. For example, much of the circumpolar tundra is dominated by bare ground in the former and by arctic grasses and boreal shrubs in the latter. Similarly, in most arid regions of the world (southwestern United States, Patagonia, Kalahari Desert, western Australia, and parts of central Asia), bare ground dominates the biome-derived PFTs while shrubs or grasses dominate the satellite-derived PFTs. Other striking differences appear in the eastern United States, where the biome-derived data show crops as the only dominant plant type while the satellite-derived data show extensive tree cover; in eastern South America, where crops are sparse in one case (biome) and abundant in the other (satellite); in southcentral Africa, where grasses are dominant according to the biome-derived data but trees are dominant according to the satellite-derived data; and in eastern Asia, where the coverage of crops and needleleaf deciduous trees differs.

3.2. Leaf Area Index

[29] The LAI phenologies for each PFT showed the expected seasonality (Figures 9 and 10). Evergreen trees had minor greening during the growing season; deciduous trees, grasses, and crops showed marked growing-season greening. Grid-average satellite LAI was different from the biome-based LAI, with differences often due to the continuous versus discrete nature of the landscape (Figure 11). However, there were distinct differences in phenology between the two data sets. For example, in the previously discussed savanna grid cell, maximum LAI is reduced somewhat between the two approaches, but the greater difference is that grasses and trees have a longer growing season in the satellite data set than the short, pronounced greening seen in the prescribed phenology of the biome data set (Figure 1). Peak LAI occurs during October compared to July and August in the biome data set. In general, the greatest differences in phenology occurred for tropical deciduous vegetation because the prescribed phenology in the biome data set adheres to a general model of summer green phenology, while the satellite data set represents observed seasonal greening.

3.3. Surface Climate

[30] The surface climate sensitivity to the biome and satellite PFT data sets was evaluated as 20-year ensemble averages for June through August and December through February. Variables of primary interest due to their direct response to changes in LAI and PFT composition include ground temperature, ground evaporation, and albedo. Other commonly considered variables (e.g., 2-m temperature, sensible heat flux, and latent heat flux) tend to confound signals from competing simulated processes (e.g., from canopy evapotranspiration versus ground evaporation or from albedo, snow cover, and soil moisture). Hence these variables are shown (Figure 12) not to explain changes between simulations but as a reminder that the changes in simulated fluxes are sometimes large and have potential implications for coupled simulations with global climate models.

3.3.1. The 3° by 3° simulations. [31] During June–August, regions with decreased grid cell average LAI had greater ground temperature (and vice versa) (Figure 13a). This warming was due to decreased shading of the ground and was partly countered by increased ground evaporative cooling (Figure 13b). Ground evaporation was greater not only as a result of higher incident solar radiation (due to lower LAI) but also as a result of reduced canopy interception of precipitation (also due to lower LAI). The latter implies more water on the ground, less on the canopy, and less canopy evaporation (Figure 13c). Less LAI produced less transpiration (Figure 13d), another direct effect which indirectly increased ground evaporation. In grid cells with large changes in ground evaporation relative to LAI changes, evaporative cooling at the ground might have reversed the shading effect and produced some of the outliers in Figure 13a. In most cases, this was a result of a concurrent change in the bare ground coverage.

[32] Because of the different definitions of bare ground between the biome PFTs and the satellite PFTs an increase in percent bare ground does not imply a decrease in grid cell average LAI (and vice versa). A change in bare ground coverage may enhance the effect of a LAI change on ground temperature and ground evaporation, or it may suppress or reverse it. However, changes in bare ground are less effective at influencing these grid cell average variables than are changes in grid cell average LAI and therefore become important only for small LAI changes (less than about ± 2 m^2 m^{-2}). Similarly, for small changes in bare ground (less than ±30%) the relationship to ground evaporation and ground temperature becomes tenuous. Generally, though, increasing the bare ground coverage tended to increase ground evaporation (Figure 13f) by lowering canopy evapotranspiration (not shown). Ground temperature was thus reduced by evaporative cooling (Figure 13e) (and vice versa when bare ground decreased). In many cases, the decrease in bare ground showed as vertical lines because in most regions (except arid and semiarid regions) the percent bare ground decreased to zero in the PFT data set from a nonzero amount for the biome data set.

[33] Cases in which changes in bare ground reversed the effects of an LAI change include the following: (1) The vertical line of outliers in Figure 13a which occurs for an LAI difference of about -2 m^2 m^{-2}, which corresponds to warm semiarid grasslands in northern Africa and the Arabian peninsula, changed from 20% bare ground in the biome simulations to almost 100% bare ground with the PFT data set. (2) The vertical line of outliers at a LAI difference of about -1 m^2 m^{-2}, which corresponds to Northern Hemisphere tundra, changed from 40% bare ground to 100% bare ground. (3) The group of outliers giving warmer ground temperature for little or no increase in LAI, which occurs where bare ground has decreased by 80% or more (various semiarid regions), is a third instance. Some cases of unchanged LAI correspond to deserts and ice sheets, where LAI is zero and bare ground cover is 100%. In these cases, ground temperature responds only to changes in albedo due to different ice cover or soil color.

[34] Model results for December–February (winter) differ from summer results only in one respect: Albedo became important in determining ground temperature in the snow-covered high-latitude

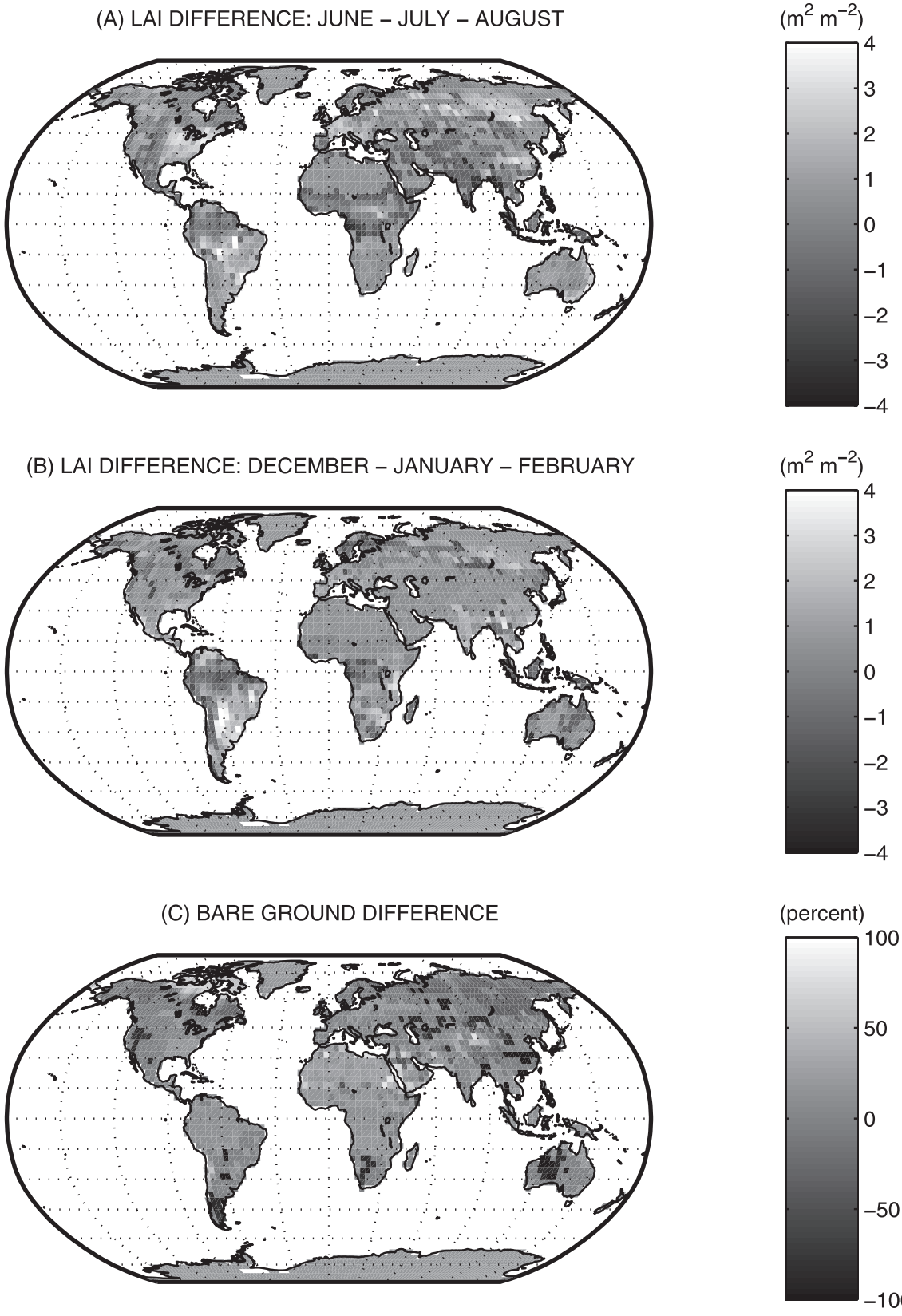

Figure 11. Vegetation differences between the satellite and biome PFT data sets (satellite minus biome). (a) June–August LAI. (b) December–February LAI. (c) Bare ground portion of grid cell. See color version of this figure at back of this issue.

forests and woodlands of the Northern Hemisphere. In this region a lower LAI reduced masking of the snow-covered ground by trees and led to higher surface albedos (Figure 14a) and cooler temperatures (Figure 14b) or vice versa for higher LAI. Elsewhere, albedo changes did not correlate with changes in LAI, and model results resembled those for June–August (Figure 14). The vertical line of cooler points with an LAI decrease of just under zero corresponds to the warm grasslands which changed to a bare ground coverage of almost 100%.

[35] The ground temperature depends on several competing nonlinear processes operating in response to changes in LAI and bare ground coverage. India and western Australia are two regions which produced outliers in Figures 13a and 13b, because reduced ground evaporation cooling prevailed over increased shading of the ground. India, during the dry monsoon, had higher LAI by $\sim$1 m^2 m^{-2} and less bare ground coverage by $\sim$20% in the PFT data set than in the biome data set. Higher LAI should increase shading of the ground, while it diminishes ground evaporation and its cooling effect. Less bare ground coverage further decreases ground evaporation. India, during the dry monsoon, is sunny and hot, with a large soil water reserve from the wet monsoon. Therefore this region is highly sensitive to a decrease in ground evaporation and results in warmer ground temperature.

[36] In western Australia the bare ground coverage changed markedly between the biome and satellite data sets. In the biome data set, western Australia was semidesert or desert with 90–100% bare ground. In the satellite data set the same region was covered mostly by broadleaf deciduous temperate shrubs (50–100%) and partly by grasses. Yet the grid average LAI difference was less than 1 m^2 m^{-2}. Increased vegetation coverage led to a higher rate of canopy evapotranspiration and much reduced ground evaporation. Soil water diminished from a combination of less water reaching the ground and more water being extracted by transpiration, so ground evaporation was further reduced, resulting in higher ground temperatures.

3.3.2. Resolution dependence. [37] The effect of changing resolution was assessed by comparing grid-average LAI for the 3° by 3°, 2° by 2°, and 1° by 1° biome-based and satellite-derived PFT data sets for four specific regions: the Amazon basin, the Mississippi basin, Australia, and eastern Siberia (Table 6). The biome PFTs are more sensitive to changes in horizontal resolution than are the satellite PFTs. For example, in the biome simulations the largest change in grid-average LAI is a 16.4% decrease during June–August in Australia from 1° to 3°. In contrast, the largest change in the satellite PFT simulations is much smaller (−8.2%), occurring in Australia during December–February. The higher sensitivity of the biome PFTs to spatial resolution than that of the satellite PFTs is expected because of the discrete versus continuous nature of the two data sets. The satellite PFTs maintain the patchiness of the landscape at each resolution, limited only by the constraint of just four PFTs in a grid cell. In contrast, the fine-scale patchiness in biome PFTs is eliminated at coarser spatial resolutions, which only allow for a single dominant biome.

4. Discussion

[38] The change from the biome to satellite PFTs resulted in large differences in the simulated energy and hydrologic budgets because of changes in the PFT composition of the grid cell, the bare ground portion of the grid cell, and LAI. Direct effects appeared in the ground temperature, ground evaporation, and the northern high-latitude winter albedo. These competing effects led to indirect effects, such as changes in soil moisture or feedbacks between temperature and latent and sensible heat fluxes. Lower resolution simulations masked landscape heterogeneity in both the biome and satellite PFTs. However, the continuous representation of vegetation in the satellite PFTs maintained more of the original landscape heterogeneity at lower resolutions compared to the biome PFTs.

[39] The satellite LAI data set must be considered preliminary and was an attempt to create a LAI data set consistent with the PFT patches. The pure PFT NDVI, which was obtained from 1-km pixels in which PFT cover was greater than 60%, is not actually pure but rather is a mix of co-occurring PFTs. The linear unmixing method was expected to give a more accurate pure PFT NDVI, but it was unstable, probably because the AVHRR data still suffer from approximate geolocation and large pixel deformation and possibly because the PFT fractions are not accurate enough at low and high tree cover. As a consequence, the phenological differences between the PFTs within a 200-km grid cell are likely to be slightly underestimated. In addition, some characteristics of the LAI data set come directly from the calibration of the LAI-NDVI relationships and from the rules used for deciduous and evergreen types, as in previous data sets [*Sellers et al.*, 1996b]. In particular, the maximum LAI expected for a PFT has a direct impact on the "mean" LAI of the data set. Because only 1 year of data is used, the interannual variability of LAI cannot be assessed, as opposed to geographic variability. Some of these limitations will be alleviated by using the Moderate-Resolution Imaging Spectroradiometer (MODIS) data set, which will have better resolution, geolocation accuracy, and validated LAI retrieval algorithm.

[40] The PFT composition of each grid cell was built from two separate and not necessarily compatible 1-km data sets of land and tree cover. The reduction in bare ground from the biome to satellite PFT data sets was a direct consequence of this inconsistency. In most cases, the non-tree-covered portion of the grid cell was not considered bare but rather covered by PFTs consistent with the land cover data set. In forests, where we knew tree cover from the tree cover data set, we could not use the corresponding land cover for the remainder because it was typically forest and we could not assume that the nontree area was bare ground. Rather, we purposely represented the nontree area as grasses, resulting in a wide geographic distribution of grasses in sparsely forested areas such as the boreal forest (Figures 7 and 8). More work is needed to merge fractional vegetation cover [e.g., *Zeng et al.*, 2000] into a consistent data set of trees, shrubs, grasses, crops, and bare ground within each 1-km pixel.

[41] The change from the biome-based to satellite-derived PFTs was motivated by a desire to provide a more accurate representation of the land surface based on the 1-km satellite data products and to better interface with ecosystem models. Landscape change can now be included by separately altering the composition and structure of PFTs within a grid cell rather than as biome replacement. Indeed, vegetation dynamics and biogeography models simulate vegetation change in terms of the abundance of PFTs [*Running and Coughlan*, 1988; *Running and Gower*, 1991; *Prentice et al.*, 1992; *Running and Hunt*, 1993; *Neilson*, 1995; *VEMAP members*, 1995; *Foley et al.*, 1996; *Haxeltine and Prentice*, 1996; *Schimel et al.*, 1997; *Kucharik et al.*, 2000].

[42] The interdisciplinary scope of PFTs raises the question of how to define PFTs that are consistent with their climate and ecosystem uses. Functional types can be derived from observations and formal classification techniques, or they can arise from a general understanding of the processes critical in determining the functioning of vegetation [*Woodward and Cramer*, 1996]. *Smith et al.* [1993] argued that PFTs should be descriptive in terms of physiological responses to environmental factors and life history characteristics required to predict vegetation response to environmental change. However, a process-based definition is inherently constrained by the processes or ecosystems under con-

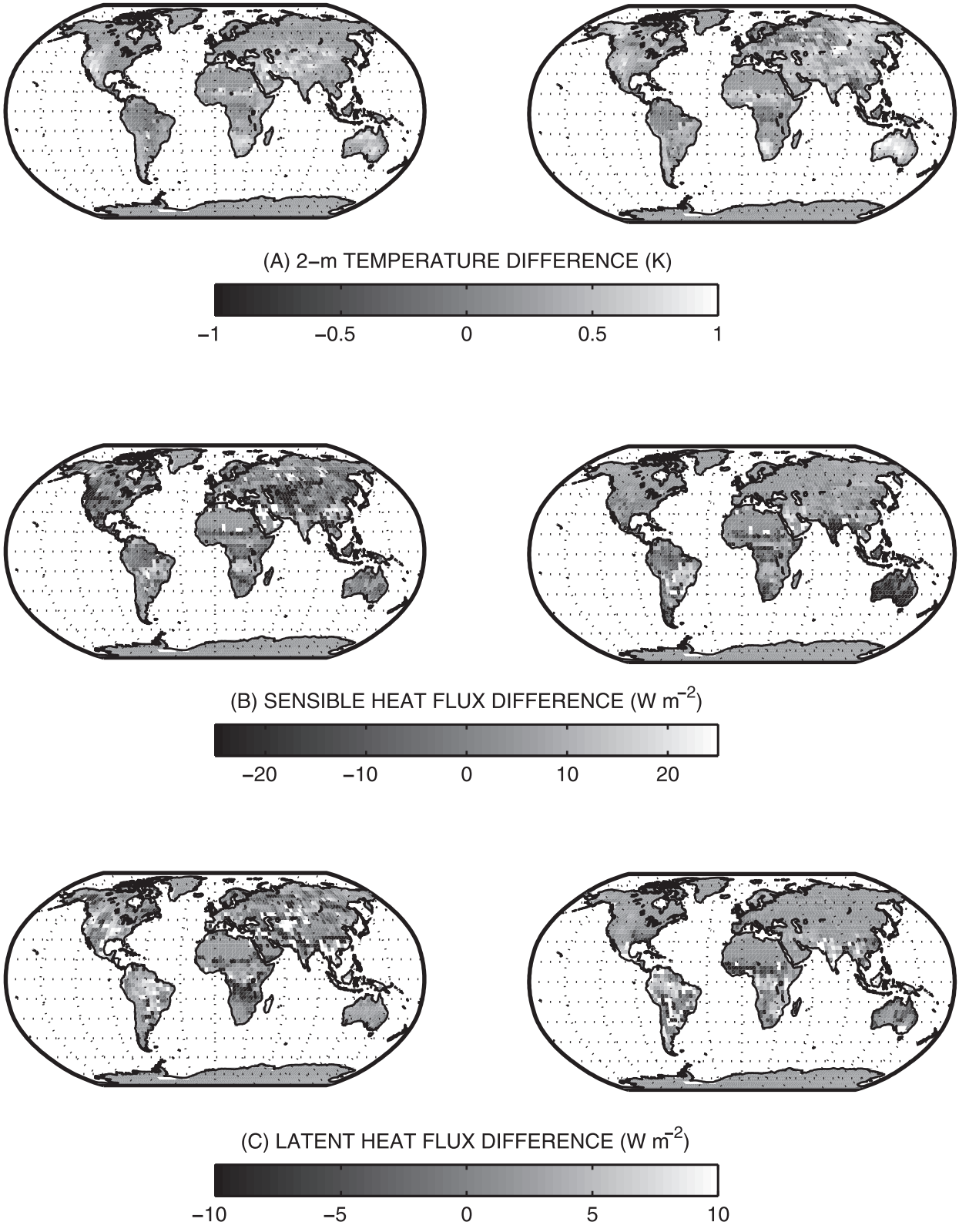

Figure 12. Differences in simulated surface variables between the satellite and biome PFT data sets (satellite minus biome) during June–August and December–February. (a) Two-meter air temperature. (b) Sensible heat. (c) Latent heat. See color version of this figure at back of this issue.

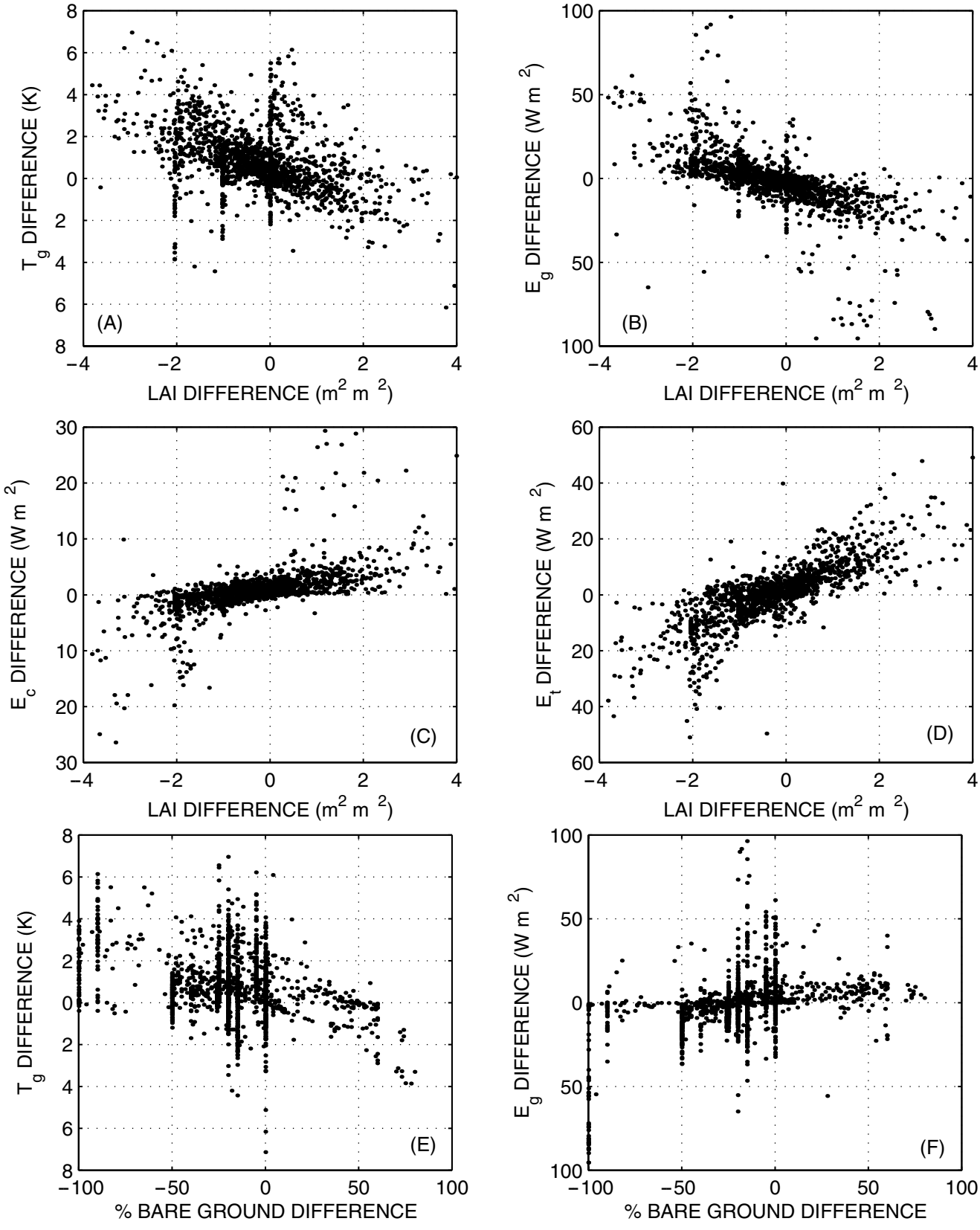

Figure 13. Scatter diagrams showing relationships between LAI and bare ground differences between the satellite and biome PFT data sets (satellite minus biome) and simulated surface variables (satellite minus biome) during June–August. (a) Ground temperature, (b) ground evaporation, (c) canopy evaporation, and (d) transpiration in relation to LAI. (e) Ground temperature and (f) ground evaporation in relation to bare ground.

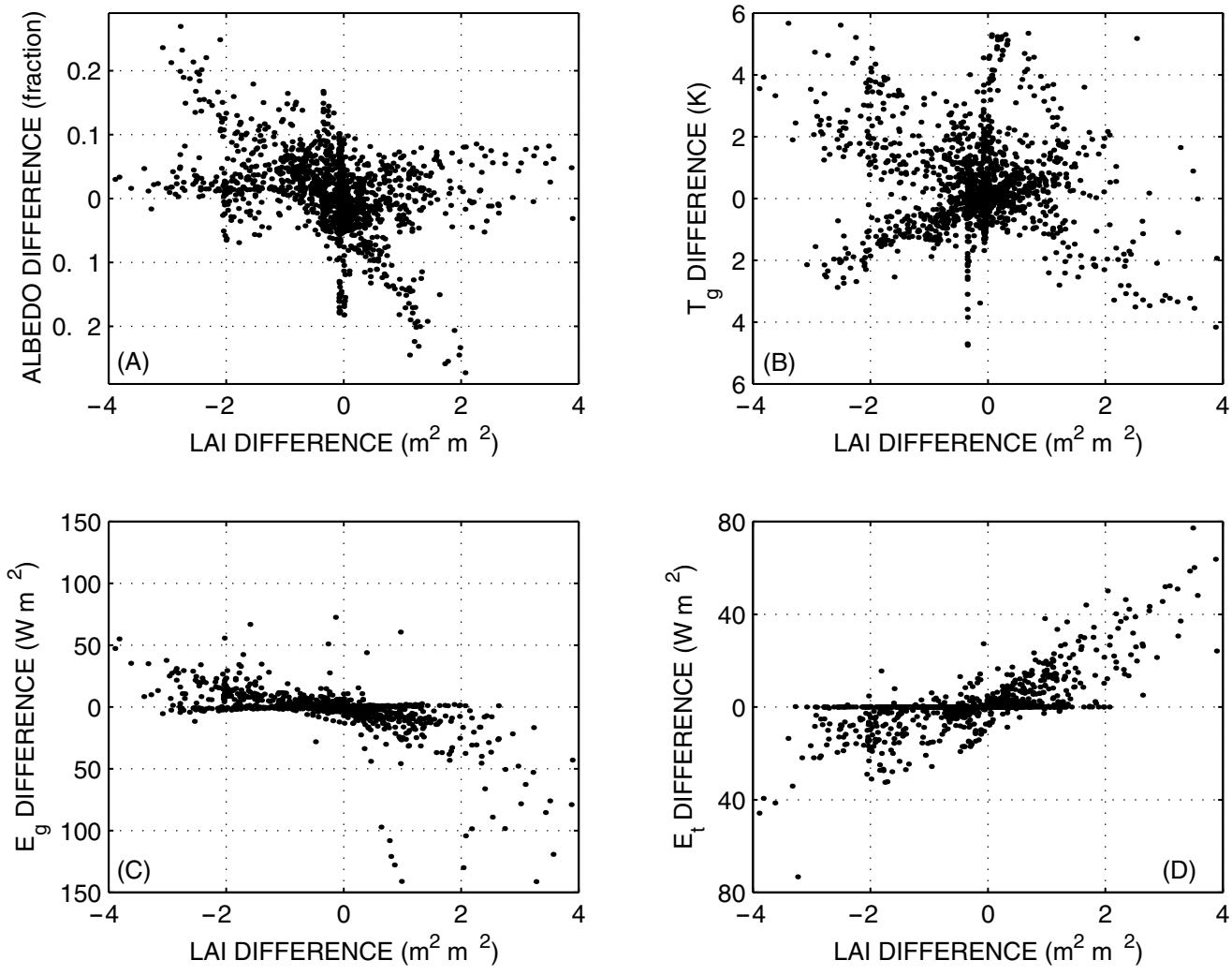

Figure 14. Scatter diagrams showing relationships between LAI differences (satellite minus biome) and surface variables (satellite minus biome) during December–February. (a) Albedo, (b) ground temperature, (c) ground evaporation, and (d) transpiration.

sideration. For example, *Box* [1996] suggested as few as 15 PFTs worldwide based on biogeographical considerations or 28 PFTs (18 woody forms, 10 nonwoody forms) based on photosynthetic and allocation patterns. Similarly, *Körner* [1993] noted that life-form, carbon allocation, physiological type, and life history characteristics are all possible means to define PFTs, each with its own utility. In the arctic, *Chapin et al.* [1996] proposed functional types based on height (tall, short), vascular or nonvascular, woody or herbaceous plant, and deciduous versus evergreen, among other factors. These determine ecological processes such as productivity, transpiration, and nutrient cycling. *Bugmann* [1996] proposed 6 PFTs for temperate and boreal forests based on four attributes: evergreen or deciduous, cold tolerance, drought tolerance, and shade tolerance. Even within a vegetation type, the number of PFTs can differ on the basis of classification considerations. *Skarpe* [1996] proposed 11 PFTs for African savannas based on, among other factors, photosynthetic pathway, rooting depth, and leaf size, type, and longevity while *Scholes et al.* [1997] arrived at 17 PFTs based on criteria such as woody or non-woody, phenology, water, herbivory, and nutrients.

[43] The combination of physiological and morphological traits along with climatic preferences may be a useful way to define plant types. Indeed, all the previous studies share this approach. The distinction between annual or perennial, evergreen or deciduous, broadleaf or needleleaf, and woody or nonwoody is a particularly useful starting point because these characteristics are observable from remote sensing and are key ecological properties determining stomatal conductance, photosynthesis, and allocation [*Running et al.*, 1995; *Nemani and Running*, 1996].

[44] One basis for this type of classification is that studies of C_3 plants growing in a wide variety of plant communities and environments and representing a diversity of life histories show correlated leaf traits such as maximum photosynthetic capacity, maintenance respiration, nitrogen concentration, leaf life span, and ratio of leaf surface area to leaf mass (specific leaf area) [*Field and Mooney*, 1986; *Reich et al.*, 1992, 1995, 1997, 1998a, 1998b; *Schulze et al.*, 1994; *Ryan*, 1991, 1995]. Maximum photosynthetic capacity and leaf respiration increase with decreasing leaf life span, increasing leaf nitrogen and increasing leaf surface area to mass ratio. Species with short-lived leaves generally have thin leaves (high specific leaf area), high leaf nitrogen, high photosynthetic capacity, high maintenance respiration, and high photosynthetic capacity per unit leaf nitrogen. Evergreen leaves, whether needleleaf or broadleaf, tend to have low photosynthetic capacity, leaf

Table 6. Resolution Dependence of Leaf Area Index in the Biome and Satellite PFT Data Sets[a]

	June–August		December–February	
	Biome PFT	Satellite PFT	Biome PFT	Satellite PFT
		Amazon Basin (9°S to 9°N and 75°W to 52°W)		
1° × 1°	3.61	3.38	3.40	2.92
2° × 2°	3.67 (1.7)	3.46 (2.4)	3.42 (0.6)	2.95 (1.0)
3° × 3°	3.95 (9.4)	3.38 (0)	3.79 (11.5)	2.90 (−0.7)
		Mississippi Basin (30°N to 45°N and 105°W to 85°W)		
1° × 1°	2.60	3.27	0.60	0.65
2° × 2°	2.59 (−0.4)	3.21 (−1.8)	0.56 (−6.7)	0.62 (−4.6)
3° × 3°	2.60 (0)	3.35 (2.5)	0.56 (−6.7)	0.66 (1.5)
		Australia (45°S to 10°S and 110°E to 160°E)		
1° × 1°	0.67	0.85	1.46	0.61
2° × 2°	0.60 (−10.5)	0.83 (−2.4)	1.38 (−5.5)	0.59 (−3.3)
3° × 3°	0.56 (−16.4)	0.81 (−4.7)	1.30 (−11.0)	0.56 (−8.2)
		Eastern Siberia (45°N to 75°N and 90°E to 180°E)		
1° × 1°	1.52	1.67	0.45	0.38
2° × 2°	1.48 (−2.6)	1.64 (−1.8)	0.41 (−8.9)	0.37 (−2.6)
3° × 3°	1.52 (0)	1.70 (1.8)	0.46 (2.2)	0.40 (5.3)

[a] Values in parentheses show the percent difference of the 2° × 2° and 3° × 3° simulations from the 1° × 1° simulation.

nitrogen, specific leaf area, and photosynthetic capacity per unit leaf nitrogen compared to deciduous trees.

[45] A physiological and morphological definition of PFTs must be reconciled with an understanding of plant responses to disturbance, which is so critical to understanding changing vegetation structure and composition. Indeed, ecologists have long characterized plants in terms of life history characteristics in relation to vegetation dynamics following disturbance: r and K strategies [*MacArthur and Wilson*, 1967; *Gadgil and Solbrig*, 1972]; early and late succession [*Bazzaz*, 1979; *Huston and Smith*, 1987]; exploitive and conservative [*Bormann and Likens*, 1979]; ruderal, stress tolerant, and competitive [*Grime*, 1979, 1993]; vital attributes that determine a plant's role in vegetation dynamics, such as method of arrival following disturbance, method of persistence during and after disturbance, and ability to establish and grow to maturity [*Noble and Slayter*, 1980]; and gap and nongap species [*Shugart*, 1984, 1987].

[46] In many cases, morphological and physiological considerations impose correlated life history traits. For example, early succession plants tend to be shade intolerant, have high rates of photosynthesis, and have high photosynthetic light compensation and saturation points. In a study of the vegetation of central western Argentina, *Díaz and Cabido* [1997] reduced a flora of 100 species to 8 PFTs based on vegetative and regenerative traits, noting a consistent trade-off between high investment in photosynthesis and growth versus preferential allocation to storage and defense. Similar trade-offs and associated traits have been reported in other types of vegetation [e.g., *Reich et al.*, 1992].

[47] **Acknowledgments.** This work was supported in part by the NASA EOS-IDS program through a grant W-19,735. The National Center for Atmospheric Research is sponsored by the National Science Foundation.

References

Bazzaz, F. A., The physiological ecology of plant succession, *Annu. Rev. Ecol. Syst.*, *10*, 351–371, 1979.

Bishop, J. K. B., W. B. Rossow, and E. G. Dutton, Surface solar irradiance from the International Satellite Cloud Climatology Project 1983–1991, *J. Geophys. Res.*, *102*, 6883–6910, 1997.

Bonan, G. B., Land-atmosphere CO_2 exchange simulated by a land surface process model coupled to an atmospheric general circulation model, *J. Geophys. Res.*, *100*, 2817–2831, 1995a.

Bonan, G. B., Sensitivity of a GCM simulation to inclusion of inland water surfaces, *J. Clim.*, *8*, 2691–2704, 1995b.

Bonan, G. B., A land surface model (LSM version 1.0) for ecological, hydrological, and atmospheric studies: Technical description and user's guide, *NCAR Tech. Note NCAR/TN-417+STR*, Natl. Cent. for Atmos. Res., Boulder, Colo., 1996.

Bonan, G. B., Effects of land use on the climate of the United States, *Climatic Change*, *37*, 449–486, 1997.

Bonan, G. B., The land surface climatology of the NCAR land surface model coupled to the NCAR Community Climate Model, *J. Clim.*, *11*, 1307–1326, 1998.

Bonan, G. B., Frost followed the plow: Impacts of deforestation on the climate of the United States, *Ecol. Appl.*, *9*, 1305–1315, 1999.

Bonan, G. B., and L. M. Stillwell-Soller, Soil water and the persistence of floods and droughts in the Mississippi River Basin, *Water Resour. Res.*, *34*, 2693–2701, 1998.

Bonan, G. B., K. J. Davis, D. Baldocchi, D. Fitzjarrald, and H. Neumann, Comparison of the NCAR LSM1 land surface model with BOREAS aspen and jack pine tower fluxes, *J. Geophys. Res.*, *102*, 29,065–29,075, 1997.

Bormann, F. H., and G. E. Likens, *Pattern and Process in a Forested Ecosystem*, 253 pp., Springer-Verlag, New York, 1979.

Box, E. O., Plant functional types and climate at the global scale, *J. Veg. Sci.*, *7*, 309–320, 1996.

Bugmann, H., Functional types of trees in temperate and boreal forests: Classification and testing, *J. Veg. Sci.*, *7*, 359–370, 1996.

Chapin, F. S., III, M. S. Bret-Harte, S. E. Hobbie, and H. Zhong, Plant functional types as predictors of transient responses of arctic vegetation to global change, *J. Veg. Sci.*, *7*, 347–358, 1996.

Coe, M. T., and G. B. Bonan, Feedbacks between climate and surface water in northern Africa during the middle Holocene, *J. Geophys. Res.*, *102*, 11,087–11,101, 1997.

Collatz, G. J., J. T. Ball, C. Grivet, and J. A. Berry, Physiological and environmental regulation of stomatal conductance, photosynthesis and transpiration: A model that includes a laminar boundary layer, *Agric. For. Meteorol.*, *54*, 107–136, 1991.

Collatz, G. J., M. Ribas-Carbo, and J. A. Berry, Coupled photosynthesis-stomatal conductance model for leaves of C_4 plants, *Aust. J. Plant Physiol.*, *19*, 519–538, 1992.

Collatz, G. J., J. A. Berry, and J. S. Clark, Effects of climate and atmospheric CO_2 partial pressure on the global distribution of C_4 grasses: Present, past, and future, *Oecologia*, *114*, 441–454, 1998.

Cowan, I. R., Stomatal behavior and environment, *Adv. Bot. Res.*, *4*, 117–228, 1977.

Cox, P. M., R. A. Betts, C. B. Bunton, R. L. H. Essery, P. R. Rowntree, and J. Smith, The impact of new land surface physics on the GCM simulation of climate and climate sensitivity, *Clim. Dyn.*, *15*, 183–203, 1999.

Craig, S. G., K. J. Holmén, G. B. Bonan, and P. J. Rasch, Atmospheric CO_2 simulated by the National Center for Atmospheric Research Community Climate Model, 1, Mean fields and seasonal cycles, *J. Geophys. Res.*, *103*, 13,213–13,235, 1998.

DeFries, R. S., J. R. G. Townshend, and M. C. Hansen, Continuous fields of vegetation characteristics at the global scale at 1-km resolution, *J. Geophys. Res.*, *104*, 16,911–16,923, 1999.

DeFries, R. S., M. C. Hansen, and J. R. G. Townshend, Global continuous fields of vegetation characteristics: A linear mixture model applied to multi-year 8 km AVHRR data, *Int. J. Remote Sens.*, *21*, 1389–1414, 2000a.

DeFries, R. S., M. C. Hansen, J. R. G. Townshend, A. C. Janetos, and T. R. Loveland, A new global 1-km dataset of percentage tree cover derived from remote sensing, *Global Change Biol.*, *6*, 247–254, 2000b.

Denning, A. S., I. Y. Fung, and D. Randall, Latitudinal gradient of atmospheric CO_2 due to seasonal exchange with land biota, *Nature*, *376*, 240–242, 1995.

Denning, A. S., G. J. Collatz, C. Zhang, D. A. Randall, J. A. Berry, P. J. Sellers, G. D. Colello, and D. A. Dazlich, Simulations of terrestrial carbon metabolism and atmospheric CO_2 in a general circulation model, part 1, Surface carbon fluxes, *Tellus, Ser. B*, *48*, 521–542, 1996a.

Denning, A. S., D. A. Randall, G. J. Collatz, and P. J. Sellers, Simulations of terrestrial carbon metabolism and atmospheric CO_2 in a general circulation model. Part 2: Simulated CO_2 concentrations, *Tellus*, *48B*, 543–567, 1996b.

Díaz, S., and M. Cabido, Plant functional types and ecosystem function in relation to global change, *J. Veg. Sci.*, *8*, 463–474, 1997.

Dickinson, R. E., A. Henderson-Sellers, and P. J. Kennedy, Biosphere-atmosphere transfer scheme (BATS) version 1e as coupled to the NCAR Community Climate Model, *NCAR Tech. Note NCAR/TN-387+STR*, Natl. Cent. for Atmos. Res., Boulder, Colo., 1993.

Dickinson, R. E., M. Shaikh, R. Bryant, and L. Graumlich, Interactive canopies for a climate model, *J. Clim.*, *11*, 2823–2836, 1998.

Dorman, J. L., and P. J. Sellers, A global climatology of albedo, roughness length, and stomatal resistance for atmospheric general circulation models as represented by a simple biosphere model (SiB), *J. Appl. Meteorol.*, *28*, 833–855, 1989.

Eidenshink, J. C., and J. L. Faundeen, The 1km AVHRR global land data set: First stages in implementation, *Int. J. Remote Sens.*, *15*, 3443–3462, 1994.

Farquhar, G. D., S. von Caemmerer, and J. A. Berry, A biochemical model of photosynthetic CO_2 assimilation in leaves of C_3 species, *Planta*, *149*, 78–90, 1980.

Field, C., and H. A. Mooney, The photosynthesis-nitrogen relationship in wild plants, in *On the Economy of Plant Form and Function*, edited by T. J. Givnish, pp. 25–55, Cambridge Univ. Press, New York, 1986.

Foley, J. A., C. I. Prentice, N. Ramankutty, S. Levis, D. Pollard, S. Sitch, and A. Haxeltine, An integrated biosphere model of land surface processes, terrestrial carbon balance, and vegetation dynamics, *Global Biogeochem. Cycles*, *10*, 603–628, 1996.

Gadgil, M., and O. T. Solbrig, The concept of r- and K-selection: Evidence from wild flowers and some theoretical considerations, *Am. Nat.*, *106*, 14–31, 1972.

Gleason, H. A., The individualistic concept of the plant association, *Bull. Torrey Bot. Club*, *53*, 7–26, 1926.

Gleason, H. A., The individualistic concept of the plant association, *Am. Midland Nat.*, *21*, 92–110, 1939.

Grime, J. P., *Plant Strategies and Vegetation Processes*, 222 pp., John Wiley, New York, 1979.

Grime, J. P., Vegetation functional classification systems as approaches to predicting and quantifying global vegetation change, in *Vegetation Dynamics and Global Change*, edited by A. M. Solomon and H. H. Shugart, pp. 293–305, Chapman and Hall, New York, 1993.

Hahmann, A., and R. E. Dickinson, A fine-mesh land approach for general circulation models and its impact on regional climate, *J. Clim.*, *14*, 1634–1646, 2001.

Haxeltine, A., and I. C. Prentice, BIOME3: An equilibrium terrestrial biosphere model based on ecophysiological constraints, resource availability, and competition among plant functional types, *Global Biogeochem. Cycles*, *10*, 693–709, 1996.

Huston, M., and T. Smith, Plant succession: Life history and competition, *Am. Nat.*, *130*, 168–198, 1987.

Idso, S. B., A set of equations for full spectrum and 8- to 14-μm and 10.5- to 12.5-μm thermal radiation from cloudless skies, *Water Resour. Res.*, *17*, 295–304, 1981.

Jones, P. D., M. New, D. E. Parker, S. Martin, and I. G. Rigor, Surface air temperature and its changes over the past 150 years, *Rev. Geophys.*, *37*, 173–199, 1999.

Kalnay, E., at al., The NCEP/NCAR 40-year reanalysis project, *Bull. Am. Meteorol. Soc.*, *77*, 437–471, 1996.

Keeley, J. E., and S. C. Keeley, Chaparral, in *North American Terrestrial Vegetation*, edited by M. G. Barbour and W. D. Billings, pp. 165–207, Cambridge Univ. Press, New York, 1988.

Knyazikhin, Y., J. V. Martonchik, R. B. Myneni, D. J. Diner, and S. W. Running, Synergistic algorithm for estimating vegetation canopy leaf area index and fraction of absorbed photosynthetically active radiation from MODIS and MISR data, *J. Geophys. Res.*, *103*, 32,257–32,276, 1998a.

Knyazikhin, Y., J. V. Martonchik, D. J. Diner, R. B. Myneni, M. M. Verstraete, B. Pinty, and N. Gobron, Estimation of vegetation canopy leaf area index and fraction of absorbed photosynthetically active radiation from atmosphere-corected MISR data, *J. Geophys. Res.*, *103*, 32,239–32,256, 1998b.

Körner, C., Scaling from species to vegetation: The usefulness of functional groups, in *Biodiversity and Ecosystem Function*, edited by E.-D. Schulze and H. A. Mooney, pp. 117–140, Springer-Verlag, New York, 1993.

Kucharik, C. J., J. A. Foley, C. Delire, V. A. Fisher, M. T. Coe, J. D. Lenters, C. Young-Molling, N. Ramankutty, J. M. Norman, and S. T. Gower, Testing the performance of a dynamic global ecosystem model: Water balance, carbon balance, and vegetation structure, *Global Biogeochem. Cycles*, *14*, 795–825, 2000.

Kutzbach, J., G. Bonan, J. Foley, and S. P. Harrison, Vegetation and soil feedbacks on the response of the African monsoon to orbital forcing in the early to middle Holocene, *Nature*, *384*, 623–626, 1996.

Legates, D. R., and C. J. Willmott, Mean seasonal and spatial variability in global surface air temperature, *Theor. Appl. Climatol.*, *41*, 11–21, 1990a.

Legates, D. R., and C. J. Willmott, Mean seasonal and spatial variability in gauge-corrected, global precipitation, *Int. J. Climatol.*, *10*, 111–127, 1990b.

Loveland, T. R., B. C. Reed, J. F. Brown, D. O. Ohlen, Z. Zhu, L. Yang, and J. W. Merchant, Development of a global land cover characteristics database and IGBP DISCover from 1 km AVHRR data, *Int. J. Remote Sens.*, *21*, 1303–1330, 2000.

Lynch, A. H., G. B. Bonan, F. S. Chapin III, and W. Wu, The impact of tundra ecosystems on the surface energy budget and climate of Alaska, *J. Geophys. Res.*, *104*, 6647–6660, 1999.

MacArthur, R. H., and E. O. Wilson, *The Theory of Island Biogeography*, 203 pp., Princeton Univ. Press, Princeton, N. J., 1967.

Myneni, R. B., R. R. Nemani, and S. W. Running, Estimation of global leaf area index and absorbed par using radiative transfer models, *IEEE Trans. Geosci. Remote Sens.*, *35*, 1380–1393, 1997.

Neilson, R. P., A model for predicting continental-scale vegetation distribution and water balance, *Ecol. Appl.*, *5*, 362–385, 1995.

Nemani, R., and S. W. Running, Implementation of a hierarchical global vegetation classification in ecosystem function models, *J. Veg. Sci.*, *7*, 337–346, 1996.

Noble, I. R., and R. O. Slayter, The use of vital attributes to predict successional changes in plant communities subject to recurrent disturbances, *Vegetatio*, *43*, 5–21, 1980.

Oleson, K. W., and G. B. Bonan, The effects of remotely sensed plant functional type and leaf area index on simulations of boreal forest surface fluxes by the NCAR land surface model, *J. Hydrometeorol.*, *1*, 431–446, 2000.

Olson, J. S., J. A. Watts, and L. J. Allison, Carbon in live vegetation of major world ecosystems, *ORNL-5862*, Oak Ridge Natl. Lab., Oak Ridge, Tenn., 1983.

Prentice, I. C., W. Cramer, S. P. Harrison, R. Leemans, R. A. Monserud, and A. M. Solomon, A global biome model based on plant physiology and dominance, soil properties, and climate, *J. Biogeogr.*, *19*, 117–134, 1992.

Randall, D. A., A revised land surface parameterization (SiB2) for atmospheric GCMs, part III, The greening of the Colorado State University general circulation model, *J. Clim.*, *9*, 738–763, 1996.

Reich, P. B., M. B. Walters, and D. S. Ellsworth, Leaf life-span in relation to leaf, plant, and stand characteristics among diverse ecosystems, *Ecol. Monogr.*, *62*, 365–392, 1992.

Reich, P. B., B. D. Kloeppel, D. S. Ellsworth, and M. B. Walters, Different photosynthesis-nitrogen relations in deciduous hardwood and evergreen coniferous tree species, *Oecologia*, *104*, 24–30, 1995.

Reich, P. B., M. B. Walters, and D. S. Ellsworth, From tropics to tundra: Global convergence in plant functioning, *Proc. Natl. Acad. Sci. U. S. A.*, *94*, 13,730–13,734, 1997.

Reich, P. B., D. S. Ellsworth, and M. B. Walters, Leaf structure (specific leaf area) modulates photosynthesis-nitrogen relations: Evidence from within and across species and functional groups, *Funct. Ecol.*, *12*, 948–958, 1998a.

Reich, P. B., M. B. Walters, D. S. Ellsworth, J. M. Vose, J. C. Volin, C. Gresham, and W. D. Bowman, Relationships of leaf dark respiration to leaf nitrogen, specific leaf area and leaf life-span: A test across biomes and functional groups, *Oecologia*, *114*, 471–482, 1998b.

Ropelewski, C. F., and M. S. Halpert, Quantifying southern oscillation-precipitation relationships, *J. Clim.*, *9*, 1043–1059, 1996.

Running, S. W., and J. C. Coughlan, A general model of forest ecosystem processes for regional applications, I, Hydrological balance, canopy gas exchange and primary production processes, *Ecol. Modell.*, *42*, 125–154, 1988.

Running, S. W., and S. T. Gower, FOREST-BGC, a general model of forest ecosystem processes for regional applications, II, Dynamic carbon allocation and nitrogen budgets, *Tree Physiol.*, *9*, 147–160, 1991.

Running, S. W., and E. R. Hunt Jr., Generalization of a forest ecosystem process model for other biomes, BIOME-BGC, and an application for global-scale models, in *Scaling Physiological Processes: Leaf to Globe*, edited by J. R. Ehleringer and C. B. Field, pp. 141–158, Academic, San Diego, Calif., 1993.

Running, S. W., T. R. Loveland, L. L. Pierce, R. R. Nemani, and E. R. Hunt Jr., A remote sensing based vegetation classification logic for global land cover analysis, *Remote Sens. Environ.*, *51*, 39–48, 1995.

Ryan, M. G., Effects of climate change on plant respiration, *Ecol. Appl.*, *1*, 157–167, 1991.

Ryan, M. G., Foliar maintenance respiration of subalpine and boreal trees and shrubs in relation to nitrogen content, *Plant Cell Environ.*, *18*, 765–772, 1995.

Schimel, D. S., and B. H. Braswell, Continental scale variability in ecosystem processes: Models, data, and the role of disturbance, *Ecol. Monogr.*, *67*, 251–271, 1997.

Scholes, R. J., G. Pickett, W. N. Ellery, and A. C. Blackmore, Plant functional types in African savannas and grasslands, in *Plant Functional Types: Their Relevance to Ecosystem Properties and Global Change*, edited by T. M. Smith, H. H. Shugart, and F. I. Woodward, pp. 255–268, Cambridge Univ. Press, New York, 1997.

Schulze, E.-D., F. M. Kelliher, C. Körner, J. Lloyd, and R. Leuning, Relationships among maximum stomatal conductance, ecosystem surface conductance, carbon assimilation rate, and plant nitrogen nutrition: A global ecology scaling exercise, *Annu. Rev. Ecol. Syst.*, *25*, 629–660, 1994.

Sellers, P. J., S. O. Los, C. J. Tucker, C. O. Justice, D. A. Dazlich, G. J. Collatz, and D. A. Randall, A global 1 by 1 degree NDVI data set for climate studies, part 2, The generation of global fields of terrestrial biophysical parameters from the NDVI, *Int. J. Remote Sens.*, *15*, 3519–3545, 1994.

Sellers, P. J., D. A. Randall, G. J. Collatz, J. A. Berry, C. B. Field, D. A. Dazlich, C. Zhang, G. D. Collelo, and L. Bounoua, A revised land surface parameterization (SiB2) for GCMs, part I, Model formulation, *J. Clim.*, *9*, 676–705, 1996a.

Sellers, P. J., S. O. Los, C. J. Tucker, C. O. Justice, D. A. Dazlich, G. J. Collatz, and D. A. Randall, A revised land surface parameterization (SiB2) for atmospheric GCMs, part II, The generation of global fields of terrestrial biophysical parameters from satellite data, *J. Clim.*, *9*, 706–737, 1996b.

Sellers, P. J., et al., Modeling the exchanges of energy, water, and carbon between continents and the atmosphere, *Science*, *275*, 502–509, 1997.

Shugart, H. H., *A Theory of Forest Dynamics*, 278 pp., Springer-Verlag, New York, 1984.

Shugart, H. H., Dynamic ecosystem consequences of tree birth and death patterns, *BioScience*, *37*, 596–602, 1987.

Skarpe, C., Plant functional types and climate in a southern African savanna, *J. Veg. Sci.*, *7*, 397–404, 1996.

Smith, T. M., H. H. Shugart, F. I. Woodward, and P. J. Burton, Plant functional types, in *Vegetation Dynamics and Global Change*, edited by A. M. Solomon and H. H. Shugart, pp. 272–292, Chapman and Hall, New York, 1993.

Smith, T. M., H. H. Shugart, and F. I. Woodward (Eds.), *Plant Functional Types: Their Relevance to Ecosystem Properties and Global Change*, 369 pp., Cambridge Univ. Press, New York, 1997.

Steinwand, D. R., Mapping raster imagery to the Interrupted Goode Homolosine projection, *Int. J. Remote Sens.*, *15*, 3463–3472, 1994.

Trenberth, K. E., The definition of El Nino, *Bull. Am. Meteorol. Soc.*, *78*, 2771–2777, 1997.

Trenberth, K. E., and T. J. Hoar, The 1990-1995 El Nino-Southern Oscillation event: Longest on record, *Geophys. Res. Lett.*, *23*, 57–60, 1996.

VEMAP members, Vegetation/ecosystem modeling and analysis project: Comparing biogeography and biogeochemistry models in a continental-scale study of terrestrial ecosystem responses to climate change and CO_2 doubling, *Global Biogeochem. Cycles*, *9*, 407–437, 1995.

Viovy, N., O. Arino, and A. S. Belward, The Best Indice Slope Extraction (BISE): A method for reducing noise in NDVI time-series, *Int. J. Remote Sens.*, *13*, 1585–1590, 1992.

Watt, A. S., Pattern and process in the plant community, *J. Ecol.*, *35*, 1–22, 1947.

Whittaker, R. H., Vegetation of the Great Smoky Mountains, *Ecol. Monogr.*, *26*, 1–80, 1956.

Woodward, F. I., and W. Cramer, Plant functional types and climatic changes: Introduction, *J. Veg. Sci.*, *7*, 306–308, 1996.

Xie, P., and P. A. Arkin, Global precipitation: A 17-year monthly analysis based on gauge observations, satelllite estimates, and numerical model outputs, *Bull. Am. Meteorol. Soc.*, *78*, 2539–2558, 1997.

Zeng, X., R. E. Dickinson, A. Walker, M. Shaikh, R. S. DeFries, and J. Qi, Derivation and evaluation of global 1-km fractional vegetation cover data for land modeling, *J. Appl. Meteorol.*, *39*, 826–839, 2000.

G. Bonan, S. Levis, and K. W. Oleson, National Center for Atmospheric Research, P. O. Box 3000, Boulder, CO 80307, USA. (bonan@ucar.edu; slevis@ucar.edu; oleson@cgd.ucar.edu)

L. Kergoat, Laboratoire d'Ecologie Terrestre, 13 av. Col. Roche, BP 4072, 31029 Toulouse cedex 4, France. (kergoat@cict.fr)

Figure 6. Biome types represented in the NCAR LSM.

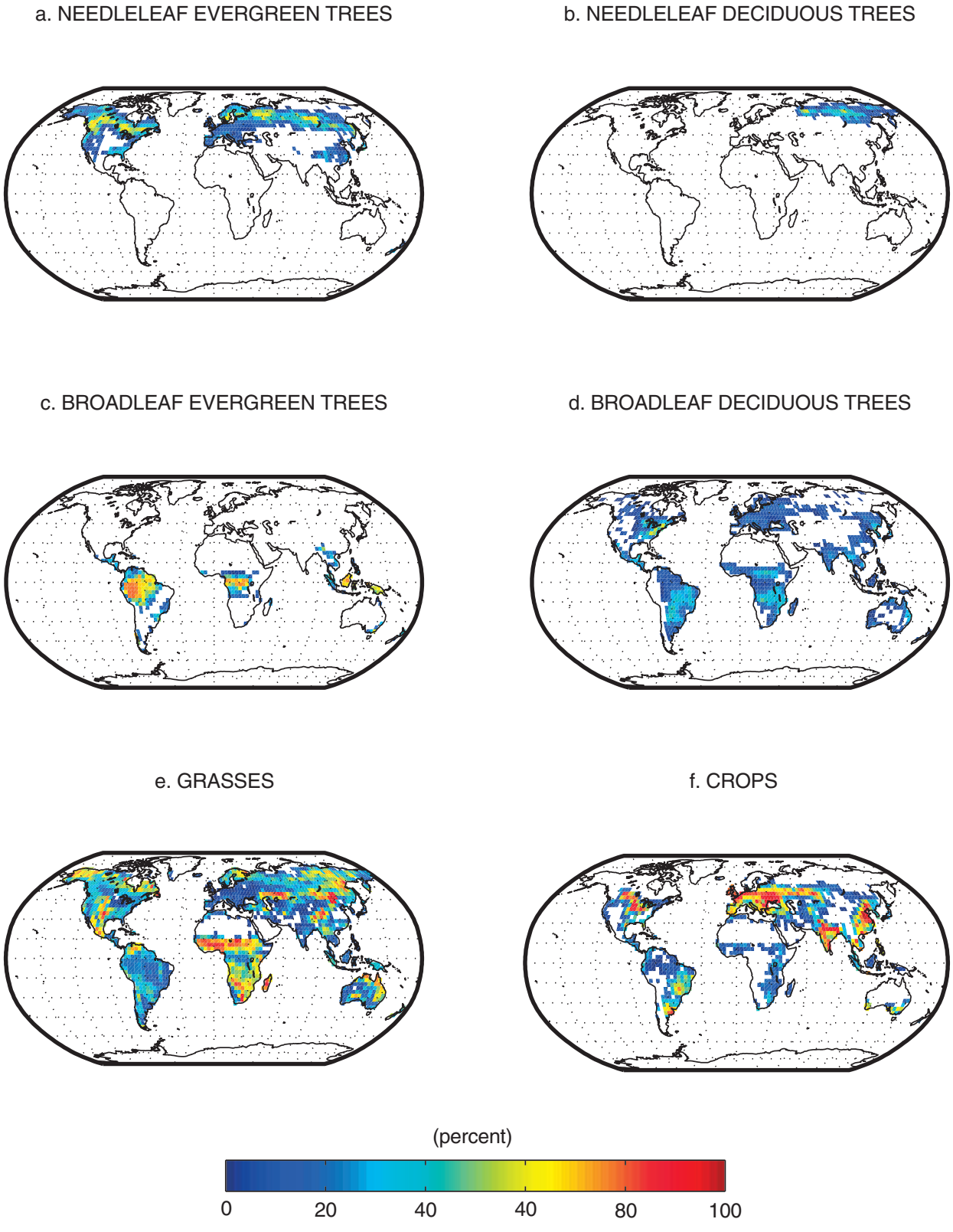

Figure 7. Distribution of (a) needleleaf evergreen trees, (b) needleleaf deciduous trees, (c) broadleaf evergreen trees, (d) broadleaf deciduous trees, (e) grasses, and (f) crops on a $3^\circ \times 3^\circ$ grid. Maps show the percent of the grid cell occupied by each plant type.

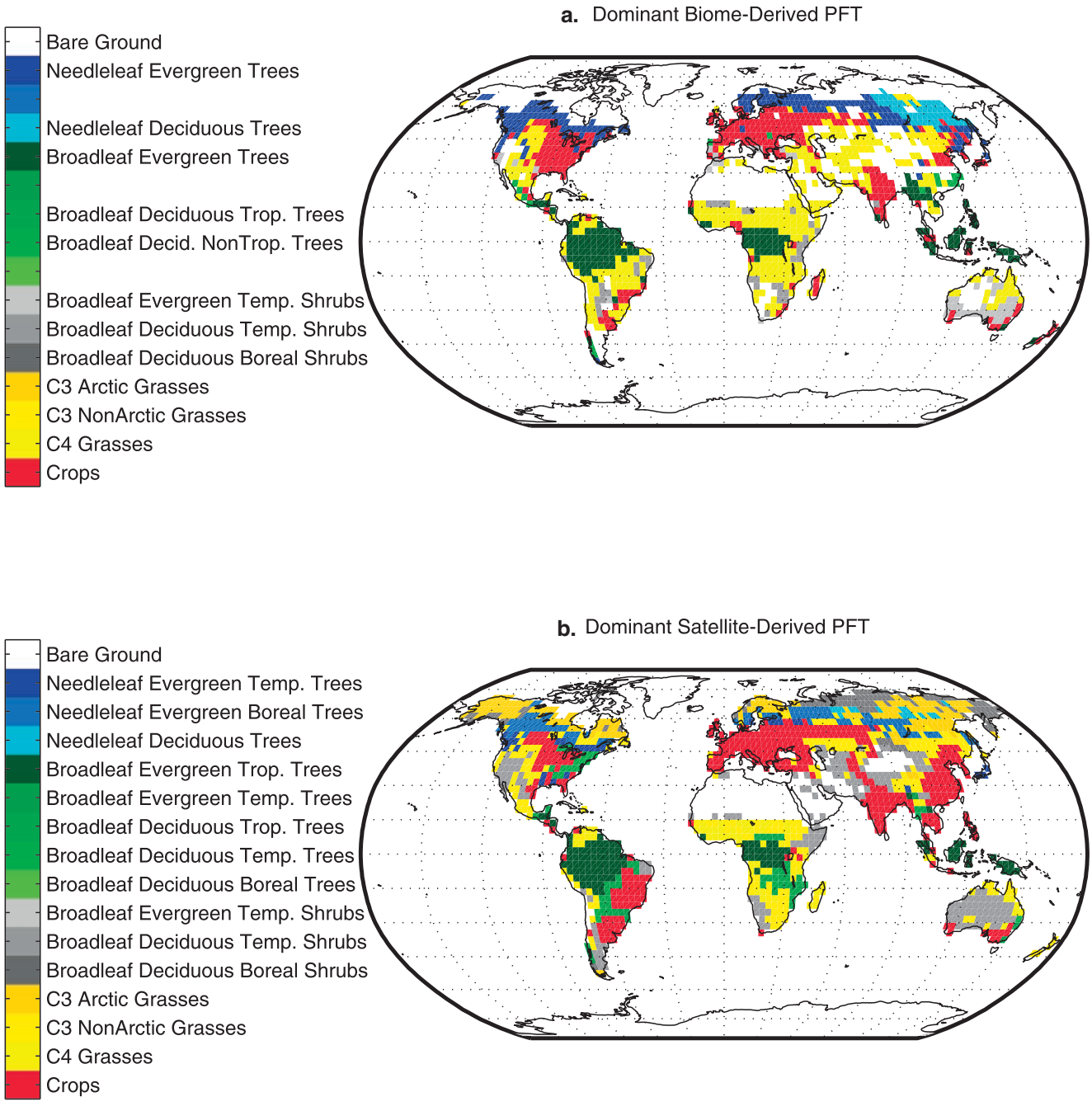

Figure 8. Dominant plant functional types. (a) Biome data set. (b) Satellite data set. See Table 3 for a definition of the PFTs.

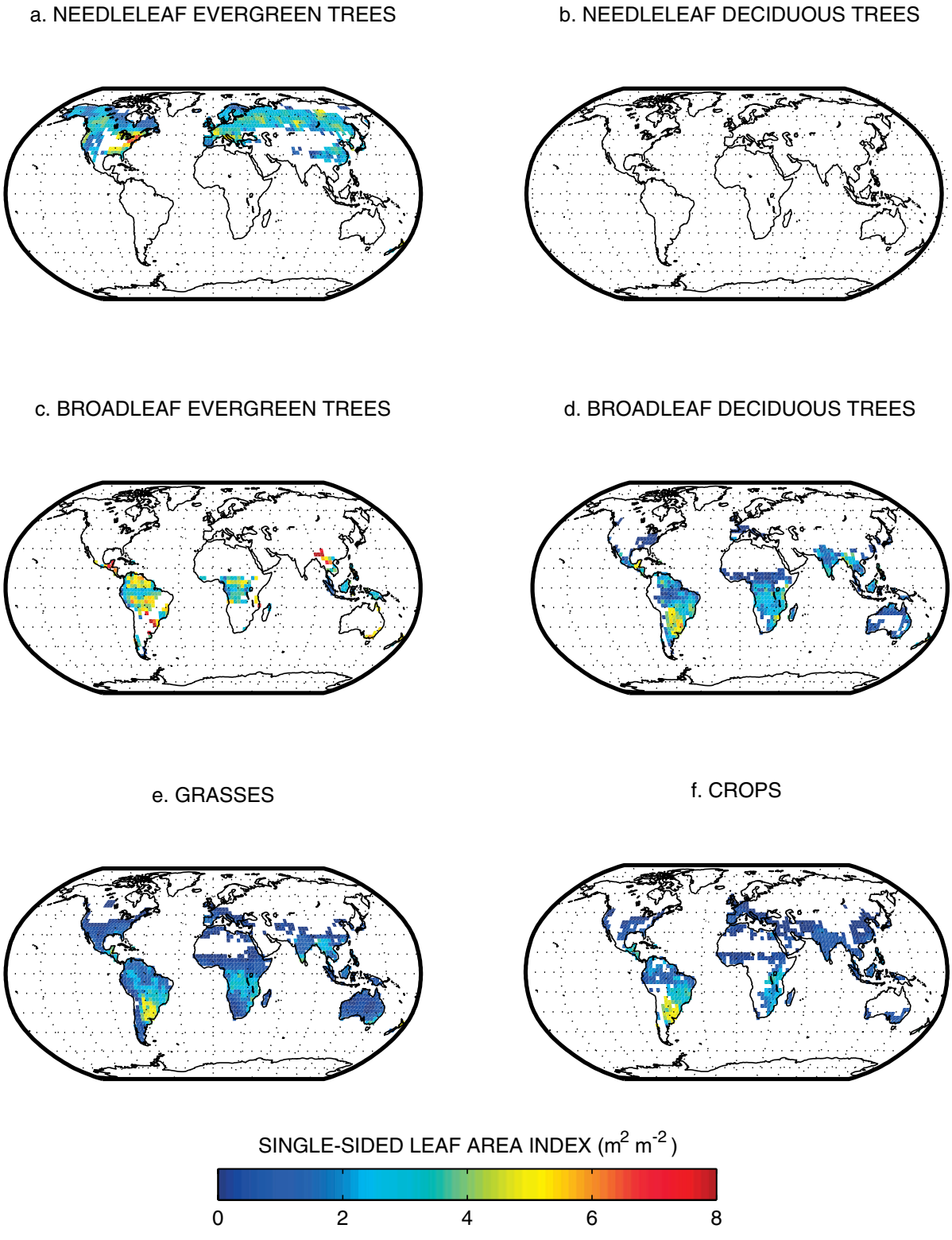

Figure 9. January satellite-derived leaf area index for (a) needleleaf evergreen trees, (b) needleleaf deciduous trees, (c) broadleaf evergreen trees, (d) broadleaf deciduous trees, (e) grasses, and (f) crops on a 3° × 3° grid.

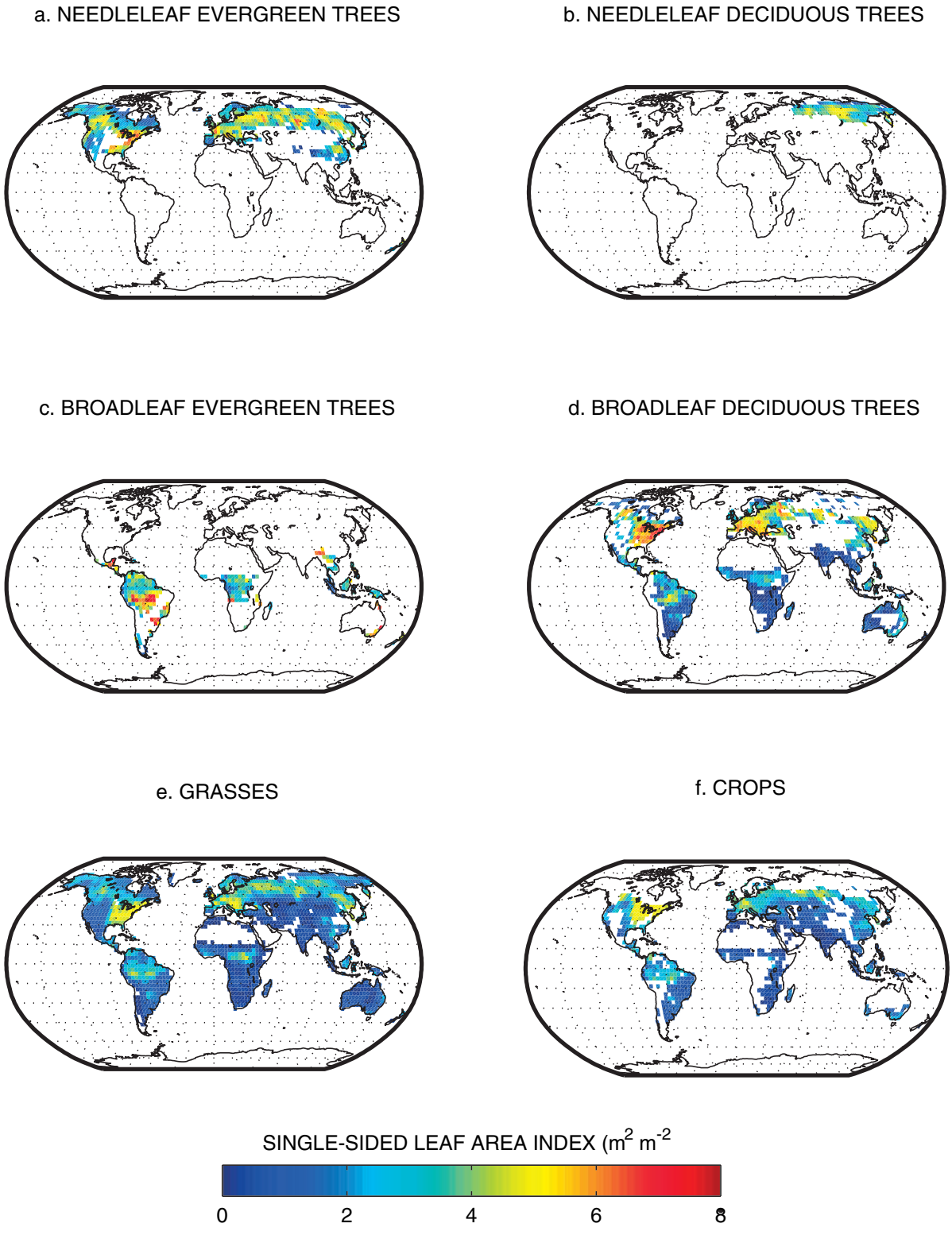

Figure 10. July satellite-derived leaf area index for (a) needleleaf evergreen trees, (b) needleleaf deciduous trees, (c) broadleaf evergreen trees, (d) broadleaf deciduous trees, (e) grasses, and (f) crops on a 3° × 3° grid.

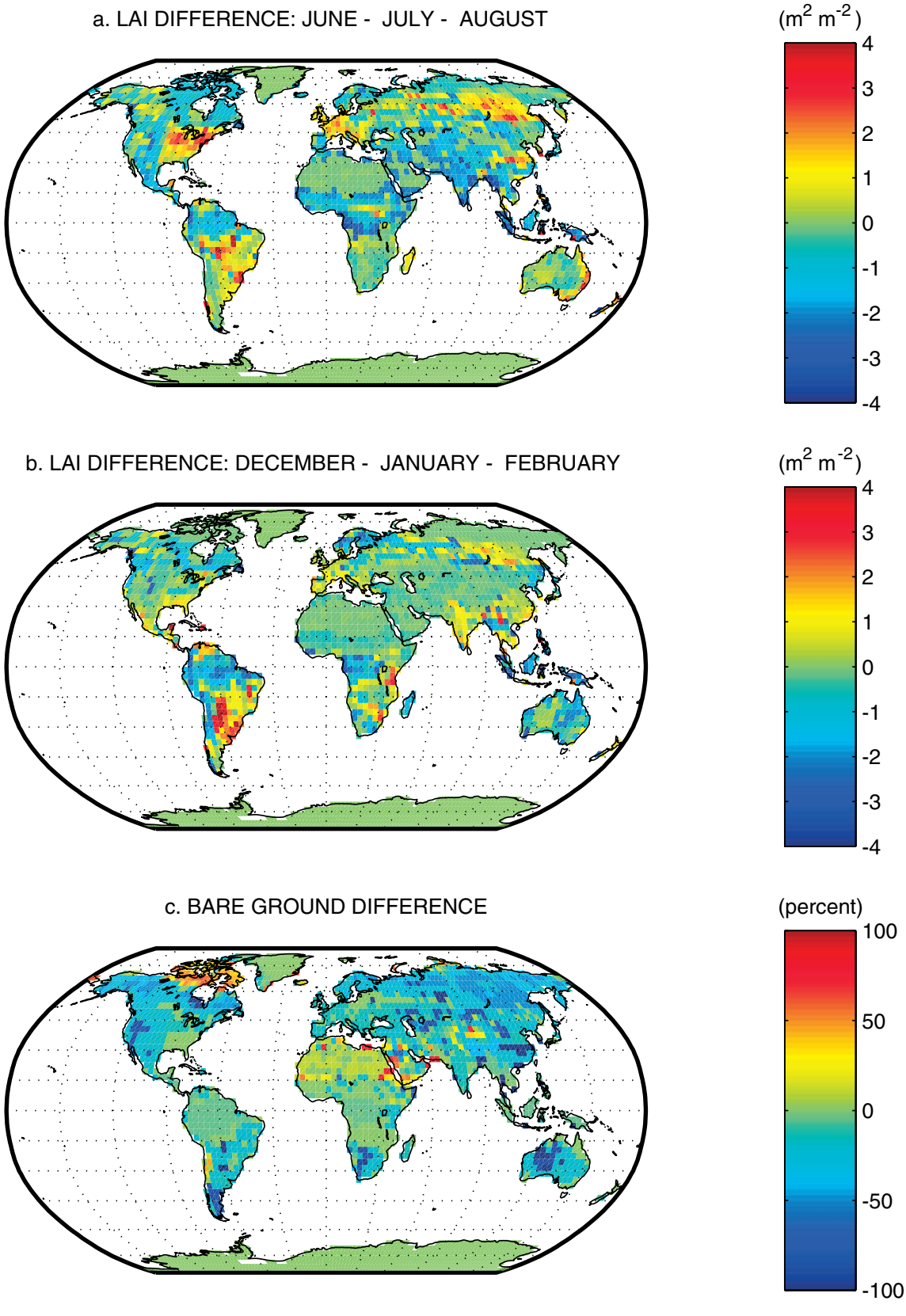

Figure 11. Vegetation differences between the satellite and biome PFT data sets (satellite minus biome). (a) June–August LAI. (b) December–February LAI. (c) Bare ground portion of grid cell.

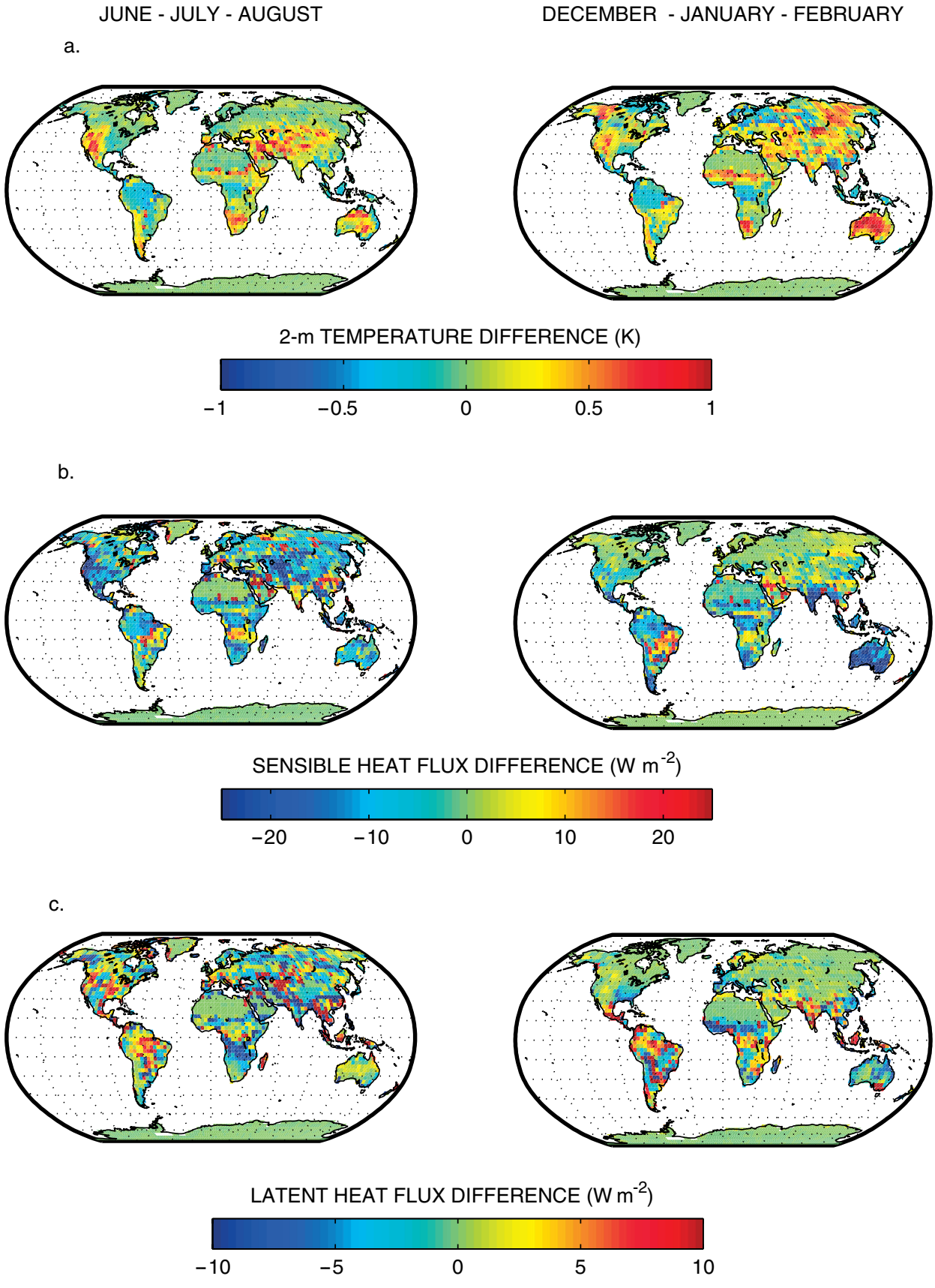

Figure 12. Differences in simulated surface variables between the satellite and biome PFT data sets (satellite minus biome) during June–August and December–February. (a) Two-meter air temperature. (b) Sensible heat. (c) Latent heat.